

# Learning Large Causal Structures from Inverse Covariance Matrix via Sparse Matrix Decomposition

Shuyu Dong<sup>\*</sup>, Kento Uemura<sup>†</sup>, Akito Fujii<sup>†</sup>, Shuang Chang<sup>†</sup>,  
Yusuke Koyanagi<sup>†</sup>, Koji Maruhashi<sup>†</sup>, and Michèle Sebag<sup>\*</sup>

<sup>\*</sup>*LISN, INRIA, Université Paris-Saclay*  
first.last@inria.fr

<sup>†</sup>*Fujitsu Laboratories Ltd.*  
first.last@fujitsu.com

February 21, 2024

## Abstract

Learning causal structures from observational data is a fundamental problem facing important computational challenges when the number of variables is large. In the context of linear structural equation models (SEMs), this paper focuses on learning causal structures from the inverse covariance matrix. The proposed method, called ICID for Independence-preserving Decomposition from Inverse Covariance matrix, is based on continuous optimization of a matrix decomposition model that preserves the nonzero patterns of the inverse covariance matrix. Through theoretical and empirical evidences, we show that ICID efficiently identifies the sought directed acyclic graph (DAG) assuming the knowledge of noise variances. Moreover, ICID is shown empirically to be robust under bounded misspecification of noise variances in the case where the noise variances are non-equal. The proposed method enjoys a low complexity, as reflected by its time efficiency in the experiments, and also enables a novel regularization scheme that yields highly accurate solutions on the Simulated fMRI data (Smith et al., 2011) in comparison with state-of-the-art algorithms.

## 1 Introduction

Discovering causal relations from observational data emerges as an important problem for artificial intelligence (Pearl, 2000; Peters et al., 2017) with fundamental and practical motivations. One notable reason is that causal models support modes of reasoning, e.g., counterfactual reasoning and algorithmic recourse (Tsirtsis et al., 2021), that are otherwise out of reach by correlation-based machine learning, as shown by Peters et al. (2016); Arjovsky et al. (2019); Sauer and Geiger (2021).

The learning of causal structures from data, also referred to as causal discovery, faces challenges in both statistical and algebraic aspects, since one needs to uncover not only correlations from data but also the underlying causal directions. In addition to difficulties related to a restricted number  $n$  of observational samples hindering the estimation process, learning a directed acyclic graph (DAG) is NP-hard (Chickering, 1996) even in the large sample limit, as the search space of DAGs increases super-exponentially with respect to the number  $d$  of variables.

**Related work.** A usual strategy to overcome computational and other difficulties is to constraint the DAG search (Spirtes et al., 2000; Meek, 1995; Chickering, 2002a; Loh and Bühlmann, 2014; Solus et al., 2021). In the linear structure equation model (SEM), Loh and Bühlmann (2014) show that the moral graph of the DAG coincides with the support graph of the inverse covariance matrix under a mild faithfulness assumption. This result entails a reduced search of DAGs within the support of the inverse covariance matrix with respect to the log-likelihood score function involving the diagonal of noise variances  $\Omega$ . Furthermore, when the true  $\Omega$  is provided, the score function admits the true DAG as the unique minimum (Loh and Bühlmann, 2014). Note however that even when  $\Omega$  is known, the actual minimum of score function is unknown, requiring a thorough search.

Another strategy for causal discovery is to formulate a continuous optimization problem based on a differentiable or subdifferentiable (e.g.,  $\ell_1$ -penalty) score function (Zheng et al., 2018; Aragam et al., 2019; Ng et al., 2020, 2021; Lopez et al., 2022). In this line of work, the optimization of the causal model, defined on the set of real square matrices, is subject to a differentiable DAG constraint (Zheng et al., 2018), or alternatively, a sparsity-promoting constraint on the sought matrix (Ng et al., 2020). The computational cost of these optimization approaches, different from combinatorial methods, depends mainly on the gradient computations which scale well enough; but the overall complexity may still be high due to the nonconvex optimization landscape (see e.g., (Zheng et al., 2018; Aragam et al., 2019)).

**Contributions.** In this paper, we present a matrix decomposition approach aimed at getting the best of both above strategies. In the linear SEM setting, the inverse covariance matrix  $\Theta$  is related to the parameters  $(B, \Omega)$  of the SEM as:

$$\Theta = (I - B)\Omega^{-1}(I - B)^T \tag{1}$$

where  $B$  is the sought causal structure and  $\Omega$  is the diagonal matrix of noise variances. Unfortunately, the above decomposition of  $\Theta$  is not unique. We show that the sought DAG  $B$  can be uniquely identified (among all feasible DAGs) through this decomposition given the true noise variance matrix  $\Omega$ . While this result takes inspiration from Loh and Bühlmann (2014), a main difference is that we use the exact matrix equation (1) for computing eligible matrix decompositions.

As the found solutions are not necessarily DAGs, the underlying optimization is augmented with an  $\ell_1$ -penalty as a sparsity-promoting term, since sparsity is shown to be an effective constraint for learning DAGs under mild assumptions on the true causal

structure (Raskutti and Uhler, 2018; Aragam et al., 2019; Ng et al., 2020). We show that, under (Ng et al., 2020, Assumptions 1–3), the  $\ell_0$  minimization subject to the matrix equality (1), achieves exact learning of linear SEMs with equal noise variances. To leverage continuous optimization, we formalize this sparse matrix decomposition problem, under the name of ICID—for Independence-preserving Decomposition from Inverse Covariance—as an equality-constrained  $\ell_1$ -minimization problem analogous to the Dantzig selector (Candes and Tao, 2007), and we tackle this problem by an augmented Lagrangian method (ALM). The computational efficiency of ICID is largely explained by our choice of restricting the nonzeros of the candidate matrix  $B$  within the support of  $\Theta$ , while the feasibility of the sought DAG is shown to be preserved. More precisely, we show that the cost of the gradient computation in ICID scales as  $O(kd^2)$  for causal models with a bounded Markov blanket size  $k$ , notably improving over NOTEARS (Zheng et al., 2018) and GOLEM (Ng et al., 2020).

Experiments (Section 4) are conducted to empirically assess the performance of ICID in causal discovery tasks compared to state-of-art methods, which show significant speedups at the expense of a moderate loss of accuracy in the linear SEM setting with equal variances (EV). Performances of ICID in learning from oracle inverse covariances are also examined, first in the EV case, and then in a challenging non-equal variance (NV) case (e.g., (Reisach et al., 2021)) with misspecifications of noise variances. Furthermore, we experiment with the Simulated fMRI dataset (Smith et al., 2011). A regularization term using skewness-based measures (Hyvärinen and Smith, 2013) is proposed and applied to ICID. The results show that the regularized ICID attains highly accurate solutions, besides DirectLiNGAM (Shimizu et al., 2011; Hyvärinen and Smith, 2013), and at the same time achieves considerable speedups over state-of-the-art methods.

## 2 Background

### 2.1 Definitions and notation

A graph  $G := (V, E)$  consists of a set of nodes  $V$  and a set of edges  $E \subset V \times V$ . Unless specified otherwise, all graphs (respectively, edges) are directed. The binary adjacency matrix of a graph  $G$  is such that its  $(i, j)$ -th entry is 1 if and only if  $(i, j) \in E$ . Conversely, any matrix  $B \in \mathbb{R}^{d \times d}$  determines an unique edge set through the nonzero entries,  $E(B) := \{(i, j) : B_{ij} \neq 0\}$ , which we also refer to as the support of  $B$ . From the definition of edge set  $E(B)$ , we assume by convention that all graphs are ordered (according to the indexing of matrix  $B$ ). The number of nonzeros of matrix  $B$  is denoted as  $\|B\|_{\ell_0}$  or  $\text{nnz}(B)$  indifferently. Given a directed acyclic graph (DAG)  $G$ , the moralization of  $G$  is defined as the undirected graph  $\mathcal{M}(G)$ , with all directed nodes in  $G$  made undirected, and new undirected edges  $(i, j)$  created for all pairs  $(i, j)$  parents of a same node  $k$ . An undirected graph is a *chordal graph* if every cycle of length greater than three has a chord, i.e., a shortcut that triangulates the cycle. For simplicity, a matrix is called a DAG (respectively, chordal) by abuse if its support graph is a DAG (resp. chordal). The set of  $d \times d$  symmetric positive definite matrices is denoted by  $\mathcal{S}_{++}^d$ . The positive definiteness

of a symmetric matrix  $\Theta$  is denoted as  $\Theta \succ 0$ .

## 2.2 Structural equation models

Structural equation models are defined on a set of random variables  $\mathbf{X} = (X_1, \dots, X_d)$ . A linear SEM  $(B, \Omega)$  expresses the causal relations among the variables as:

$$\mathbf{X} = B^T \mathbf{X} + \mathbf{N} \quad (2)$$

where matrix  $B \in \mathbb{R}^{d \times d}$  is supported on a DAG  $G$  and  $\mathbf{N} = (\epsilon_1, \dots, \epsilon_d)$  is a vector of  $d$  noise variables. Here, the variables  $\mathbf{X}$  and  $\mathbf{N}$  are assumed to be centered and that  $\epsilon_j \perp\!\!\!\perp X_i$  for all  $i \in \text{PA}_j^G$  where  $\text{PA}_i^G$  is the set of parent nodes of  $X_i$  in  $G$ . The joint distribution  $P_{\mathbf{X}}$  satisfies the Markov property with respect to  $G$ , and its density function can be factorized as  $p(\mathbf{x}) = \prod_{i=1}^d p(x_i | x_{\text{PA}_i^G})$ .

Since  $\mathbf{X}$  and  $\mathbf{N}$  are centered and  $\epsilon_j \perp\!\!\!\perp X_i$  for all  $i \in \text{PA}_j^G$ , the covariance of  $\mathbf{N}$  is a diagonal matrix  $\Omega := \text{diag}(\omega_1^2, \dots, \omega_d^2)$ , where  $\omega_i^2$  denotes the variance of  $\epsilon_i$ . The linear SEM (2) with the DAG  $B$  entails that  $\mathbf{X} = (I - B)^{-1} \mathbf{N}$  since  $(I - B)$  is invertible. Consequently, the covariance matrix of  $\mathbf{X}$  is  $\text{cov}(\mathbf{X}) = (I - B)^{-T} \Omega (I - B)^{-1}$ , and the inverse covariance matrix (or the precision matrix) of  $\mathbf{X}$  reads:

$$\Theta := \varphi(B, \Omega^{-1}) = (I - B) \Omega^{-1} (I - B)^T. \quad (3)$$

The property above yields the following result. As Theorem 2 shows, the nonzero patterns (or edge set  $E(\Theta)$ ) of the inverse covariance matrix is in fact a subset of the moralized graph of  $B$ .

**Lemma 1** (Loh and Bühlmann (2014)). *Let  $\mathbf{X}$  be a random variable following the SEM (2) of  $(B, \Omega)$ . Then the coefficients of the inverse covariance matrix  $\Theta$  of  $\mathbf{X}$  are as follows, for all  $i$  and  $j \neq i$  in  $[d]$ :  $\Theta_{ij} = -\frac{B_{ij}}{\omega_j^2} - \frac{B_{ji}}{\omega_i^2} + \sum_{\ell=1}^d \frac{B_{i\ell} B_{j\ell}}{\omega_\ell^2}$ , and  $\Theta_{ii} = \frac{1}{\omega_i^2} + \sum_{\ell=1}^d \frac{B_{i\ell}^2}{\omega_\ell^2}$ .*

**Theorem 2** (Loh and Bühlmann (2014)). *The inverse covariance matrix  $\Theta$  (3) reflects the graph structure of the moralization  $\mathcal{M}(B)$  through inclusion: for  $i \neq j$ ,  $(i, j)$  is an edge in  $\mathcal{M}(B)$  if  $\Theta_{ij} \neq 0$ .*

The converse of Theorem 2 is not always true but is considered as a mild assumption (Assumption 3), stating that any edge  $(i, j)$  in  $\Theta$  yields either a directed edge, or the existence of a common child, between  $i$  and  $j$  in  $B$ . This condition is a type of faithfulness assumption Koller and Friedman (2009); Spirtes et al. (2000).

**Assumption 3** (Loh and Bühlmann (2014)). *Let  $\mathbf{X}$  be a random variable following the SEM of  $(B, \Omega)$ . The inverse covariance matrix  $\Theta$  (3) of  $\mathbf{X}$  satisfies, for all  $i \neq j$ ,  $\Theta_{ij} = 0$  only if  $B_{ji} = B_{ij} = 0$  and  $B_{i\ell} B_{j\ell} = 0$  for all  $\ell$ .*

### 3 Independence-preserving decomposition of the precision matrix

Taking inspiration from Loh and Bühlmann (2014); Ghoshal and Honorio (2018), we consider the causal discovery problem with the linear SEM in a two-step framework: i) estimating the inverse covariance matrix  $\Theta$  (3) of  $\mathbf{X}$  from observational data (statistical part); ii) recovering a causal structure matrix  $B$  from  $\Theta$  (structural learning part). We study the second, structural learning part assuming  $\Theta$  is given by an oracle or estimated from observational data.

#### 3.1 Matrix decomposition within a sparse support

Given an inverse covariance matrix  $\Theta$ , the matrix equation (Eq. 3) generally admits multiple DAG solutions, and the set of solutions becomes even larger without the DAG constraint on  $B$ . From the results in Section 2, however, it is possible to reduce the vast solution set by considering a restriction on the candidate support graph. Assumption 3 ensures that the non-zero pattern (or edge set) of  $\Theta$  coincides with the moralization of  $B$ . This allows us to define a matrix decomposition model more specific than (3), which we call a *support-constrained* decomposition.

**Definition 4.** Let  $\Theta \in \mathcal{S}_{++}^d$  be a positive definite matrix. The set  $\mathcal{S}(\Theta)(\Theta)$  is defined as the set of pairs of matrices  $(B, D)$ , where  $B \in \mathbb{R}^{d \times d}$  and  $D \succ 0$  is a strictly positive diagonal matrix, such that:

$$\mathcal{S}(\Theta) := \{(B, D) : \Theta = (I - B)D(I - B)^T, \text{diag}(B) = \mathbf{0}, D \succ 0, \text{ and } E(B) \subset E(\Theta)\}. \quad (4)$$

A pair  $(B, D)$  realizes a *support-constrained* decomposition of  $\Theta$  if it belongs to  $\mathcal{S}(\Theta)$ . The domain of  $B$  corresponding to the support constraint is denoted as

$$E_\Theta := \{B \in \mathbb{R}^{d \times d} : \text{diag}(B) = \mathbf{0}, E(B) \subset E(\Theta)\}. \quad (5)$$

The support-constrained decomposition is always well-defined in the case of chordal matrices. In fact, the set  $\mathcal{S}(\Theta)$  is nonempty when  $\Theta \succ 0$  is supported on a chordal graph; see Proposition 8 (in Appendix A.1).

In the general case where  $\Theta$  is not a chordal matrix, then  $\mathcal{S}(\Theta)$  contains the sought solution under Assumption 3:

**Proposition 5.** *Let  $\Theta$  be the inverse covariance matrix of  $\mathbf{X}$  obeying the linear SEM with  $(B, \Omega)$ , i.e.,  $\Theta = \varphi(B, \Omega)$  (3). Suppose that this SEM satisfies Assumption 3, then the set  $\mathcal{S}(\Theta)$  contains  $(B, \Omega^{-1})$ .*

The proof to this proposition, and the proof of all results in this section are given in Appendix A.

In addition to the sought solution  $(B, \Omega)$ ,  $\mathcal{S}(\Theta)$  also contains pairs  $(B', \Omega')$  for  $B'$  Markov equivalent to  $B$ . Ghassami et al. (2020) shows the specific rotations  $Q$  that realize

the transformation from  $(I - B)$  to  $(I - B')$  and  $\Omega$  to  $\Omega' \succ 0$  such that  $\varphi(B', \Omega') = \varphi(B, \Omega)$ . Moreover, for any  $B'$  Markov equivalent to  $B$ ,  $\mathcal{M}(B) = \mathcal{M}(B')$  which coincides with  $E(\Theta)$ . Hence  $B'$  also satisfies the support constraint regarding the set (4). In particular, we show next that any DAG  $B$  such that  $(B, \Omega^{-1})$  belongs to the set (4) with the true noise variances matrix  $\Omega$ , is the sought true causal structure:

**Theorem 6.** *Let  $(B^*, \Omega^*)$  be a linear SEM satisfying Assumption 3 and let  $\Theta = \varphi(B^*, \Omega^*)$  be the inverse covariance of  $\mathbf{X}$  following this SEM. If a DAG  $B \in \mathbb{R}^{d \times d}$  is such that  $(B, \Omega^{*-1}) \in \mathcal{S}(\Theta)$ , then  $B = B^*$ .*

The result of Theorem 6, similar to (Loh and Bühlmann, 2014, Theorem 7), requires the knowledge of the noise variances. (Loh and Bühlmann, 2014, Theorem 7) supported causal discovery through a DAG enumeration approach. In our case, Theorem 6 supports a causal discovery approach based on a novel sparse matrix decomposition method.

### 3.2 ICID model learning via constrained optimization

Theorem 6 suggests searching for a DAG that realizes the support-preserving matrix decomposition of  $\Theta$ . One way to tackle this challenging task is by relaxing the DAG constraint and minimizing the number of edges (nonzeros of  $B$ ) subject to the constraint that  $\varphi(B, D) = \Theta$ :

$$\underset{B \in E_\Theta, D \succ 0}{\text{minimize}} \|B\|_{\ell_0} \quad \text{subject to} \quad (I - B)D(I - B)^T = \Theta \quad (6)$$

where the search space  $E_\Theta$  of  $B$  is defined in (5). Noting that the constrained set (4) contains at least one DAG (Proposition 5), the  $\ell_0$  minimization helps the selection by discarding graphs with cycles, since cycles usually implies redundant edges from spurious causal directions. The following corollary, deduced from Theorem 6 and (Ng et al., 2020, Theorem 1), supports this claim in the case with equal noise variances (EV case) under a generalized faithfulness assumption and a causal minimality condition (Ghassami et al., 2020; Ng et al., 2020).

**Corollary 7.** *Let  $\mathbf{X}$  be a variable following a linear SEM  $(B^*, \Omega^*)$ . Suppose the precision matrix  $\Theta$  of  $\mathbf{X}$  satisfies the Assumptions 1–2 of Ng et al. (2020), and that the noise variances are equal. Then, as long as the skeleton of  $B^*$  does not contain any triangle, the  $\ell_0$  minimization (6) has a unique global optimum  $(B, D)$  where  $D_{ii} \equiv \min_{j \in [d]} \{\Theta_{jj}\}$  and  $B = B^*$ .*

To benefit from the  $\ell_0$  minimization effects while leveraging continuous optimization techniques for matrix decomposition, we resort to the following matrix decomposition problem:

$$\underset{B \in E_\Theta, D \succ 0}{\text{minimize}} \|B\|_{\ell_1} \quad \text{subject to} \quad (I - B)D(I - B)^T = \Theta \quad (7)$$

where  $\|B\|_{\ell_1} := \sum_{i,j} |B_{ij}|$  is a continuous relaxation of  $\ell_0(B)$  for limiting the number of nonzeros in the solution, and the search space  $E_\Theta$  of  $B$  is defined in Eq. 5.

The  $\ell_1$  minimization problem (7) is analogous to the Dantzig selector (Candes and Tao, 2007) for high-dimensional statistical problems. Combined with an inverse covariance estimator, this problem (7) yields a method for causal discovery from observational data. In the context of causal structure learning, we use the term *independence-preserving decomposition* (ICID) to refer to problem (7). Note that the locations of the zeros of  $\Theta$  encode the independence relations within  $\mathbf{X}$  (in the Gaussian setting, (Loh and Bühlmann, 2014, Remark 3)), thus the preservation of the independent pairs after the decomposition, i.e.,  $\{(i, j) : \Theta_{ij} = 0\} \subset \{(i, j) : B_{ij} = 0\}$ , corresponds exactly to the support constraint  $E(B) \subset E(\Theta)$  of the problem (7).

**Additional regularization.** The ICID problem (7) is deduced from the linear SEM without restriction on the distributions of the  $\mathbf{X}$  and  $\mathbf{N}$  variables (Section 2.2). Therefore the ICID approach is open to the possibility of additional regularization schemes depending on the specific properties of the variable and noise distributions. In cases where the data distributions are skewed, for example, the third-order cumulant statistics carry important information of the pairwise causal directions (Hyvärinen and Smith, 2013). Taking this inspiration, we introduce a skewness-based regularization for ICID as follows,

$$\underset{B \in E_\Theta, D \succ 0}{\text{minimize}} \quad \|B\|_{\ell_1} + \lambda_2 \text{tr}(\tilde{M}^\top (B \odot B)) \quad \text{subject to} \quad (I - B)D(I - B)^\top = \Theta, \quad (8)$$

$$\text{where} \quad \tilde{M} := -C_{\mathbf{X}} \odot \mathbb{E}[\mathbf{X}g(\mathbf{X})^\top - g(\mathbf{X})\mathbf{X}^\top]. \quad (9)$$

Here  $C_{\mathbf{X}}$  denotes the correlation matrix of  $\mathbf{X}$  and  $g(\cdot)$  applies to  $\mathbf{X}$  elementwisely. For skewed distributions, we take  $g(x) = -x^2$  in the spirit of (Hyvärinen and Smith, 2013, Theorem 2); details are given in Appendix B.4.

The algorithms described in the next subsection are meant to solve problem (7) and its regularized formulation (8).

### 3.3 Algorithm

As the ICID problems (7) and (8) are nonconvex and nonsmooth (since the feasible set of the matrix equation  $\varphi(B, D) = \Theta$  is nonconvex and the  $\ell_1$ -term in the objective is nonsmooth), we consider the augmented Lagrangian method (ALM) (Bertsekas, 1999) to solve them. Algorithm 1 presents the procedure for optimizing the augmented Lagrangian of ICID. The presented algorithm assumes the equal variance setting ( $\Omega$  is a multiple of the identity matrix). Under this assumption, the sought solution  $B$  can be retrieved in light of Corollary 7.<sup>1</sup>

The equality constraint of ICID consists of  $\frac{d(d+1)}{2}$  equalities. Let  $\Lambda$  be the  $d \times d$  matrix of the Lagrange multipliers for these equalities. Then the augmented Lagrangian of ICID given  $D$  is

$$L^\rho(B; \Lambda) = f(B) + \langle \Lambda, \Theta - \varphi(B, D) \rangle + \frac{\rho}{2} \|\Theta - \varphi(B, D)\|_{\mathbb{F}}^2 \quad (10)$$

---

<sup>1</sup>It will be shown experimentally on real-world data that the algorithm can also yield good performances in the general case, when the equal noise variance assumption is not guaranteed.

where  $f(B) := \|B\|_{\ell_1}$  for problem (7) and  $f(B) := \|B\|_{\ell_1} + r(B)$  with  $r(B) = \lambda_2 \text{tr}(\tilde{M}^T(B \odot B))$  for problem (8).

---

**Algorithm 1** ALM for ICID with a fixed diagonal  $D$

---

**Input:** Inverse covariance matrix  $\Theta$ , parameters  $\beta \in (0, 1)$ ,  $\rho_0 > 0$ , tolerance  $\epsilon > 0$

**Output:**  $B_t \in E_\Theta$

1: **Initialize:**  $B_0 \leftarrow \mathbf{0}$ ,  $\Lambda_0 \leftarrow \mathbf{0}$ ,  $\rho \leftarrow \rho_0$ , and  $D_{ii} \leftarrow \min_{j \in [d]} \{\Theta_{jj}\}$  for all  $i \in [d]$ .

2: **for**  $t = 1, \dots, \mathbf{do}$

3:   **Primal descent:** for  $L^\rho(B; \Lambda)$  defined in (10), compute # see Algorithm 2  
     (Appendix B.1)

$$B_t = \arg \min_{B \in E_\Theta} L^\rho(B; \Lambda_{t-1}) \quad (11)$$

    with  $\rho \geq \rho_0$  such that  $\mathcal{I}_t := \|\Theta - \varphi(B_t, D)\|_F \leq \beta \mathcal{I}_{t-1}$

4:   **Dual ascent:**  $\Lambda_t \leftarrow \Lambda_{t-1} + \rho(\Theta - \varphi(B_t, D))$

5:   **if**  $\|\Theta - \varphi(B_t, D)\|_F \leq \epsilon$  **then**   return  $B_t$  as solution

6: **end for**

---

The efficiency of Algorithm 1 mostly depends on the resolution of the primal descent problem (line 3; Eq. (11)). For this reason, an adaptation of the FISTA (Beck and Teboulle, 2009) is designed (Algorithm 2, Appendix B.1) according to the structure of the primal problem (11). The adaptation is in the computation of the gradient descent stepsize, which is based on an efficient second-order approximation of the line minimization of (the smooth part of)  $L^\rho(B; \Lambda_{t-1})$ . Details are given in Appendix B.1 (see Eq. (26)).

**Computational cost.** The dominant cost of Algorithm 2 corresponds to the computation of the gradient  $\nabla_B \tilde{L}^\rho(\cdot, \Lambda)$  at each iteration, where  $\tilde{L}^\rho(\cdot, \Lambda)$  denotes the smooth part of  $L^\rho(\cdot, \Lambda)$ . As Proposition 10 (Appendix B) shows, given the support constraint of  $B$ , this gradient computation only requires  $O(kd^2)$  floating-point operations, where  $k$  is the maximal node degree of the graph of  $\Theta$  (which equals the maximal Markov blanket size of the true DAG under Assumption 3).

This contributes to the efficiency of the proposed algorithm. Indeed, as long as the maximal Markov blanket size of the true DAG is upper-bounded by a constant  $k$  independent of the graph size  $d$ , then the per-iteration cost of Algorithm 2 is bounded by  $O(d^2)$ , which is greatly reduced compared to other continuous optimization-based approaches.

**Discussion.** It is worth noting that ICID does not rely on any estimation of a causal ordering for learning matrix  $B$ , as opposed to ordering-based methods (Ghoshal and Honorio, 2018; Chen et al., 2019; Gao et al., 2022). However, a causal ordering estimated from a solution  $B$  of ICID can be used in an ordering-based matrix decomposition approach, using e.g., Cholesky decomposition of  $\Theta$  or (Ghoshal and Honorio, 2018, Algorithm 1), for yielding potentially improved candidate solutions. Such a combination of ICID with ordering-based matrix decomposition approaches is left for further work.



## 4 Experiments

We conduct experiments on synthetic and real-world data to assess the performance of ICID in causal structure learning from inverse covariance matrices and also in causal discovery tasks. The primary goal of the experiments is to examine the learning accuracy of the proposed method and its computational efficiency in different settings.

The proposed algorithms are available at <https://github.com/shuyu-d/icid-v2>.

### 4.1 Experimental setting

**Benchmark data.** Following Zheng et al. (2018), the synthetic data are generated from linear SEMs where the causal structure  $B$  is drawn from the Erdős–Rényi (ER) or the scale-free (SF) (Barabási and Albert, 1999) random graphs. The coefficients (edge weights) of  $B$  are drawn from the uniform distribution  $\text{Unif}([-2, -0.5] \cup [0.5, 2])$ . Experiments are also conducted on the Simulated fMRI dataset (Smith et al., 2011).

**Baselines.** The ICID method is tested in two scenarios. One scenario is to assess the proposed causal learning methodology irrespective of the statistical issues of inverse covariance estimation, in which case ICID is exceptionally labeled as  $\mathcal{O}$ -ICID, meaning that the precision matrix  $\Theta$  is the ground truth one. The other scenario is causal discovery, in which case ICID takes as input a precision matrix learned from observational data using a sparse inverse covariance estimator (details in Algorithm 4, Appendix B.3).

In the benchmarks,  $\mathcal{O}$ -ICID is tested along with (Ghoshal and Honorio, 2018, Alg. 1)—labeled as GH18—which is also given the ground truth  $\Theta$  as input. Both methods are compared with GES (Chickering, 2002b) and its Java-based implementation fastGES (Ramsey et al., 2017), which take the observational data as input. ICID is compared with DirectLINGAM (Shimizu et al., 2011), ICA-LINGAM (Shimizu et al., 2006), GES/fastGES, NOTEARS (Zheng et al., 2018) and GOLEM (Ng et al., 2020). The estimated graphs are evaluated by usual metrics (SHD, TPR, FDR and FPR) (details in Appendix C.2).

The CPU-based methods are run on one CPU of Intel(R) Xeon(R) Gold 5120 14 cores @ 2.2GHz; GOLEM is run on a GPU of Tesla V100-PCIE-32GB.

### 4.2 Scalability in causal discovery

In this experiment, ICID is evaluated in causal discovery tasks, in comparison with NOTEARS, GOLEM and GES / FastGES, on random DAGs within the ER1 set with equal variance noise. The number  $d$  of nodes varies in  $\{100, 200, 400, 600, 800, 1000, 2000\}$ , and the number of samples of  $\mathbf{X}$  is set as  $n = 10d$ . The performances of  $\mathcal{O}$ -ICID (provided with the ground truth  $\Theta$ ) are also reported to showcase the structural learning aspect of ICID.

The optimization parameters of ICID, selected after a simple tuning using grid search, are given in Appendix B.1. In this benchmark, ICID uses a single ALM iteration (Algorithm 1) followed by a projection on the DAG space for eliminating cycles (details in Appendix B.2).  $\mathcal{O}$ -ICID uses multiple ALM iterations with respect to an accuracy-based

stopping criterion (details in Appendix B.1). ICID and NOTEARS use the same CPU resource, similar to fastGES, and GOLEM is run on GPU.

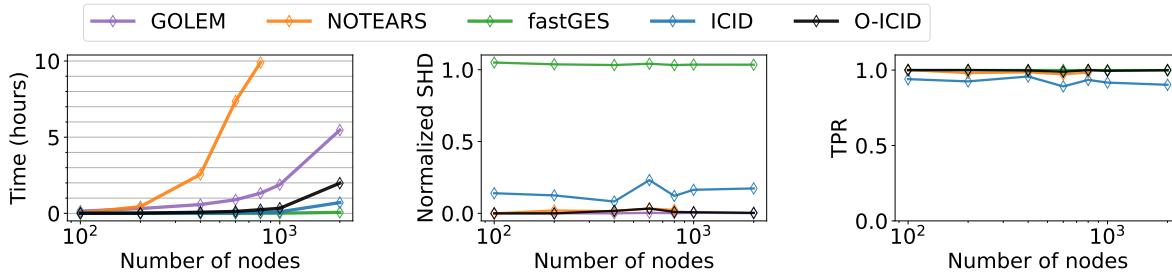


Figure 1: Causal discovery results vs number of nodes. The number of nodes  $d$  range from 100 to 2000. The SHD scores in the middle subplot are normalized by  $\text{nnz}(B^*)$ .

The results in Figure 1 show that ICID scales up efficiently—with a 5 times speedup over GOLEM for  $d = 2000$ ; and even greater speedups over NOTEARS for  $d \geq 600$ ), at the expense of a moderate loss in terms of TPR (above 80%) and the normalized SHD (below 20%). ICID outperforms fastGES in terms of SHD, within a comparably low computation time in all settings of  $d$ .  $\mathcal{O}$ -ICID yields close-to-exact learning accuracy in both TPR and SHD—besides GOLEM—while demonstrating good scalability.

### 4.3 Learning from the precision matrices and robustness

In this experiment, we further examine the structural learning part of ICID (Algorithm 1) given oracle precision matrices, namely  $\mathcal{O}$ -ICID. The linear SEMs are generated for the EV case and a NV case described as follows.

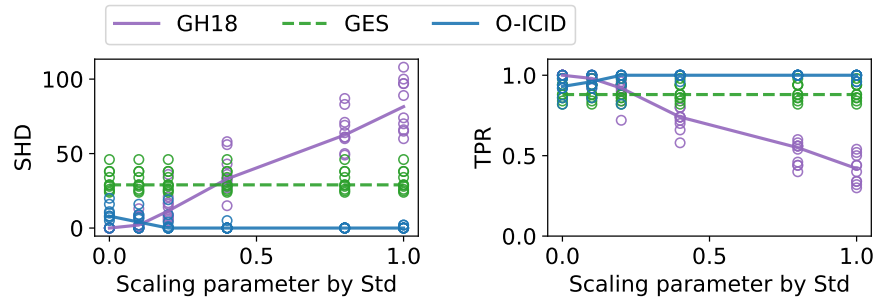
Given a linear SEM variable  $\mathbf{X}$  with equal noise variances, let  $D_u$  be the diagonal matrix such that  $(D_u)_{ii} = \sqrt{\text{var}(X_i)}$ , and consider the following family of SEMs:

$$\mathbf{X}^{(\lambda)} := D_u^{-\lambda} \mathbf{X} \quad \text{for } 0 < \lambda \leq 1. \quad (12)$$

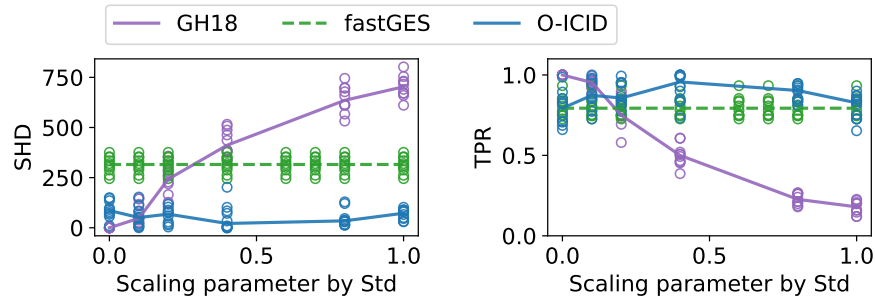
It can be shown that  $\mathbf{X}^{(\lambda)} = (D_u^{-\lambda} B D_u^\lambda)^\top \mathbf{X}^{(\lambda)} + D_u^{-\lambda} \mathbf{N}$ . The noise variance matrix of  $\mathbf{X}^{(\lambda)}$  is  $\tilde{\mathbf{N}} = D_u^{-\lambda} \mathbf{N}$ , which has a diagonal covariance matrix  $\tilde{\Omega} = D_u^{-\lambda} \Omega D_u^{-\lambda} = D_u^{-2\lambda}$ ; note that  $\mathbf{X}^{(1)}$  is the standardization of  $\mathbf{X}$ .

In the first study, in light of Theorem 6, we evaluate the effectiveness of  $\mathcal{O}$ -ICID in the NV ( $\lambda > 0$ ) case, given the true noise variances. Hence  $\mathcal{O}$ -ICID is tested using the oracle diagonal matrix  $D^* := \tilde{\Omega}^{-1}$  (overriding  $D$  in Algorithm 1, line 1) when  $\lambda > 0$ . The EV ( $\lambda = 0$ ) case is also tested as a reference. The baseline method GH18 is tested using the same inverse covariance matrices, and GES (and/or fastGES) are tested using the observational data. For each setting of  $\lambda \in \{0, 0.1, 0.2, 0.4, 0.8, 1.0\}$ , the methods are evaluated with 10 random linear SEMs on ER $k$  DAGs ( $k = 1, 2, 3$ ). The number of nodes is  $d = 50$ .

The results in Figure 2 (a)–(b) (on ER1 and ER3) show that  $\mathcal{O}$ -ICID and GH18 reach close-to-exact or exact learning accuracy (with often zero SHDs) for very small values of



(a) ER1



(b) ER3

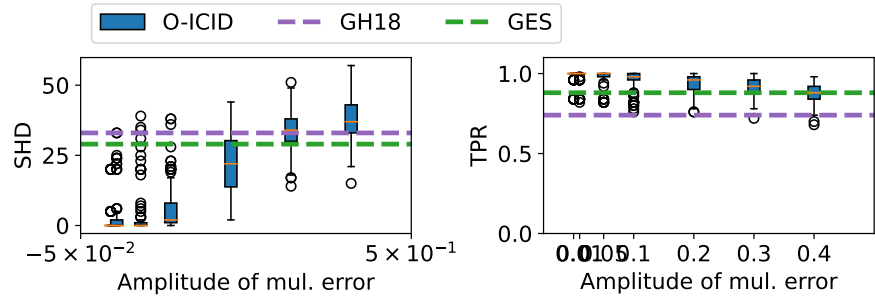
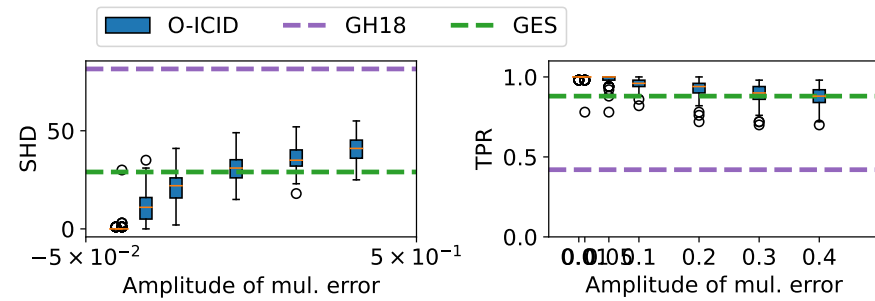
(c) ER1,  $\lambda = 0.4$ (d) ER1,  $\lambda = 1$ 

Figure 2: Causal structure learning by  $\mathcal{O}$ -ICID compared to GH18 and GES. The true DAGs are drawn from the ER1 and ER3 sets with  $d = 50$  nodes. In (a)–(b): the x-axis indicates the scaling parameter  $\lambda$  in (12). In (c)–(d): the SHD plots use the log scale for the x-axis of  $\sigma$  while the TPR plots use the linear scale for the same values of  $\sigma$ .

$\lambda$ , corresponding to the EV case. When  $\lambda$  increases, however, the baselines of GH18 are seriously degraded for  $\lambda \geq 0.4$ . We notice that this is due to the fixed, variance-based node ordering rule of GH18, which is tailored for the EV case (and cases with small  $\lambda$ ); see (Ghoshal and Honorio, 2018, Assumption 1). By contrast,  $\mathcal{O}$ -ICID (with the true noise variances given) remains stable and almost insensitive to  $\lambda$ . Such stability is observed on all ER $k$  graphs tested. The stability of  $\mathcal{O}$ -ICID on SF2 and SF4 graphs is satisfactory in the sense that it has better or comparable accuracy than the baselines of GES for all  $\lambda$ . The complete set of results are detailed in Appendix C.3. These observations suggest the effectiveness of the proposed Algorithm 1 for ICID given the true noise variances.

The computation time for  $\mathcal{O}$ -ICID is around 1 to 3 seconds (Tables 5 and 6, in Appendix C.3) on the ER $k$  graphs, which is comparable to fastGES (for ER3) and slightly longer than GH18, respectively, and is much shorter than GES, as could be expected from their theoretical complexities.

**Misspecification of  $D$ .** The second study considers the NV case where Algorithm 1 is provided with a corrupted noise variance matrix  $\hat{D}$ . The misspecification of  $\hat{D}$  is parametrized by multiplicative error terms: for all  $i \in [d]$  independently,  $\hat{D}_{ii} := \max(\frac{1}{2}, 1 + \epsilon)\tilde{\Omega}_{ii}^{-1}$ , with  $\epsilon \sim \mathcal{N}(0, \sigma)$  for  $\sigma \in (0, \frac{1}{2})$ , where the minimal value  $\frac{1}{2}$  in the multiplicative term is a safeguard to ensure positive definiteness of  $\hat{D}$ . The results are reported for  $\sigma$  in  $\{0, 0.01, 0.05, 0.1, 0.2, 0.3, 0.4\}$ , in Figure 2 (c)–(d). For ER1,  $\lambda = 0.4$ , a relatively challenging NV case (in view of Figure 2 (a)), the comparisons in Figure 2 (c)–(d) show that  $\mathcal{O}$ -ICID outperforms the baselines (the dashed lines marking the average scores) of GH18 and GES within moderate multiplicative misspecifications ( $\sigma \leq 0.2$ ) in terms of SHD and TPR. Similar comparisons (Figures 8 and 9, in Appendix C.3) are observed with other settings on ER $k$  graphs.

## 4.4 Experiments on Simulated fMRI Data

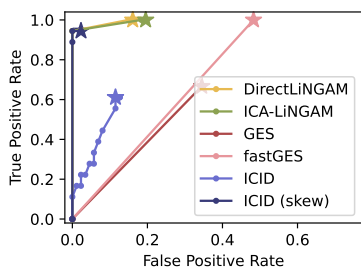
The simulations of the fMRI time series are described in detail by Smith et al. (2011). Networks of varied complexity were used to simulate fMRI timeseries. The simulations were based upon the dynamic causal modelling (DCM) forward model (Friston et al., 2003). DCM uses the nonlinear balloon model (Buxton et al., 1998) for the vascular dynamics, that is, the connection between the neural activities and the measured signal, sitting above a simple neural network model of the neural dynamics. The nodes of the DCM corresponded to brain regions. The external binary inputs (encoding neural activations) to the nodes are generated, which are not the same as the noise variables in the SEM, although related. Neural noise of standard deviation 0.05 of the difference in height between the two states was added. Different simulation datasets (Sim1–Sim28, (Smith et al., 2011, Table 1)) were generated depending on parameters including the number of nodes, duration of the fMRI session, and the number of separate realizations (“subjects”).

The causal discovery methods are examined on Sim3 ( $d = 15$  nodes) and Sim4 ( $d = 50$ ), respectively, using all subjects’ time series as observational data. The regularized ICID problem (8), labeled as ICID (skew), is motivated by the prior knowledge on the fMRI

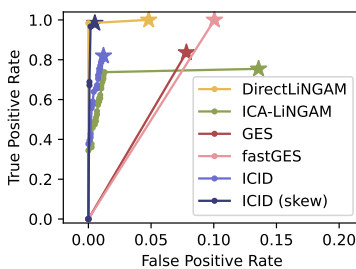
data that its skewness is mainly positive (Hyvärinen and Smith, 2013, §2.9). Specifically, the matrix  $\tilde{M}$  (9) in the regularization term of ICID (skew) is defined with a third-order cumulant-based pairwise measure (Hyvärinen and Smith, 2013, Theorem 2), and the choice of  $g(x) := -x^2$  in (9) reflects the prior knowledge about the skewness of the fMRI data. More details including the Sim3 and Sim4 datasets, and the parameter selection of ICID (skew) are given in Appendix B.4.

Table 1: Causal discovery results on the fMRI Sim4 data (Smith et al., 2011).

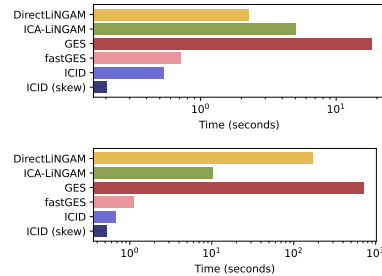
<i>fMRI Sim4</i>	SHD	TPR	FDR	FPR	time (seconds)
DirectLiNGAM	56	1.0	0.479	0.048	168.722
ICA-LiNGAM	158	0.754	0.775	0.136	10.307
GES	90	0.836	0.641	0.078	709.984
fastGES	89	1.0	0.657	0.101	1.121
ICID	14	0.820	0.219	0.012	0.679
ICID (skew)	<b>6</b>	0.984	<b>0.090</b>	<b>0.005</b>	<b>0.517</b>



(a) fMRI Sim3



(b) fMRI Sim4



(c) Running time

Figure 3: Results on the Simulated fMRI datasets (Sim3 and Sim4): (a)–(b) ROC curves. (c) Running time on Sim3 (upper) and Sim4 (lower).

The performances of ICID and ICID (skew) on the Sim4 data, together with the baselines of DirectLiNGAM, ICA-LiNGAM, GES and fastGES, are reported in Table 1. Moreover, on Sim3 and Sim4, each method is evaluated through the ROC curves of their estimated graphs, given in Figure 3 (a)–(b), together with the running time in Figure 3 (c). The results show that ICID obtains the second best SHD score (after ICID (skew)) on Sim4, with a good trade-off between the TPR and the FDR, and a computation time lower than fastGES. Moreover, on Sim3 and Sim4, ICID (skew) recovers almost exactly the true DAGs (attaining the lowest SHDs and close-to-one TPRs)—besides DirectLiNGAM—with a significantly low computation time.

## 5 Discussion

The two approaches most related to ICID are that of Loh and Bühlmann (2014) and Ghoshal and Honorio (2018) as all rely on the inverse covariance matrix, yielding an

identifiability result provided the knowledge of the noise variances. The main difference regards the algorithmic approaches. Loh and Bühlmann (2014) proceed by defining a likelihood-based score on DAG structures, and then by searching for its minimizer using dynamic programming, assuming that the support graph of  $\Theta$  has a restricted tree-width. Ghoshal and Honorio (2018) proceed iteratively, recovering a topological order that is consistent with the causal structure. At each iteration a terminal variable is determined and removed from the linear SEM, while the corresponding row of the causal DAG is deduced using (3).

The difference between ICID and (Loh and Bühlmann, 2014) is twofold. On one hand, ICID tackles a decomposition of the inverse covariance matrix subject to a support constraint. Algorithm 1 thus addresses a constrained continuous optimization problem (7); an adapted FISTA is used in the ALM of Algorithm 1, which has a significantly reduced computational cost due to the support constraint in (7). On the other hand, ICID enables to check the optimality of the provided solution (via the matrix equality constraint) while the approach in (Loh and Bühlmann, 2014) requires an exhaustive enumeration of the candidate solutions. ICID offers the same identifiability guarantees as (Loh and Bühlmann, 2014, Theorem 7) under the same assumptions, as shown in Theorem 6 and supported empirically in Section 4.3.

Likewise, the difference between ICID and (Ghoshal and Honorio, 2018) lies in the algorithmic strategies. The complexity of GH18 (Ghoshal and Honorio, 2018, Alg. 1) is lower than ICID; however GH18 primarily depends on the consistency of its topological ordering rule (based on variances), which holds under (Ghoshal and Honorio, 2018, Assumption 1). In the general case where this assumption does not hold, e.g., in challenging NV cases, the accurateness of GH18 is seriously degraded, while ICID (namely  $\mathcal{O}$ -ICID) shows better robustness as empirically evidenced in Section 4.3.

Another related work, Varando (2020) tackles the decomposition of the inverse covariance matrix through (3) and maximum-likelihood of the linear SEM. ICID differs mainly in that it uses the support constraint in the formulation of problem (7) and exploits this constraint in its optimization.

A more remotely related approach is that of maximum-likelihood estimation (MLE) based methods (Aragam et al., 2019; Ng et al., 2020). Note that the log-likelihood function for inverse covariance estimation (via the Graphical Lasso formulation (Friedman et al., 2007)) can be rewritten in terms of the linear SEM parameters  $(B, \Omega)$  with  $\Theta$  as in (3). It follows that, ignoring the constant terms,  $\frac{1}{2}f(\Theta; X) := \frac{1}{2n} \text{tr}(X^T \Theta X) - \frac{1}{2} \log \det(\Theta) = -\log p(B, \Omega; X)$ , which is the M-estimator of GOLEM (Ng et al., 2020) for optimizing  $B$ . The difference between ICID and GOLEM is that ICID proceeds with two separate steps, which in total are computationally lighter than the MLE approach of GOLEM. ICID has a lower per-iteration cost than GOLEM. Overall, it is suggested and empirically supported that ICID offers an improved scalability than GOLEM (Section 4.2).

## 6 Conclusion and perspectives

This main contribution of the paper is the ICID method that decomposes the inverse covariance matrix  $\Theta$  for learning causal structures. ICID leverages continuous optimization techniques for decomposing  $\Theta$  subject to a support constraint (7). This approach (paired with a basic, empirical inverse covariance estimation method) demonstrated high efficiency in learning causal structures on both small and large graphs, and showed good scalability up to thousands of nodes. The ICID approach thus offers the potential to leverage future advances regarding the inverse covariance estimation step, noting that this step faces some of the key challenges (regarding, e.g., node degree distributions of the sought DAG, limited amount of observational data) for causal discovery.

Perspectives for further research include design of regularization schemes, and ensemble approaches on the top of ICID, e.g., considering solutions obtained with different candidates for the inverse noise variance matrix  $D$ . The question of whether and how these solutions can be exploited will be investigated by taking inspiration from the Cause-Effect Pair Challenge (Guyon et al., 2019), leveraging supervised learning on the top of candidate solutions, to learn classifiers (dedicated to the considered graphs) discriminating the true edges from the spurious ones.

## A Proofs

### A.1 Example with chordal matrices

The following theorem illustrates the well-definedness of the support-constrained decomposition (Definition 4) in the case where  $\Theta$  is supported on a chordal graph. This result builds upon the characterization of Cholesky decomposition of positive definite matrices supported on a chordal graph (Fulkerson and Gross, 1965; Rose, 1970; Paulsen et al., 1989; Vandenberghe and Andersen, 2015).

**Proposition 8.** *Let  $\Theta \in \mathcal{S}_{++}^d$  be a positive definite matrix whose support graph  $E(\Theta)$  is chordal. Then  $\Theta$  admits a support-constrained decomposition (Definition 4). More over, the set  $\mathcal{S}(\Theta)$  (4) contains a pair  $(B, D)$  where  $B \in \mathbb{R}^{d \times d}$  is supported on a DAG.*

*Proof.* For completeness, we state the following lemma on the connections between chordal graphs and positive definite matrices that can *factor without fill* (Fulkerson and Gross, 1965; Rose, 1970; Paulsen et al., 1989). Given an undirected graph  $G = (V, E)$  endowed with a node ordering  $\sigma$ , the following sets are considered:

$$\mathcal{S}_{G,\sigma} = \{\Theta \in \mathcal{S}_{++}^d : \Theta_{ij} = 0 \text{ for } (\sigma^{-1}(i), \sigma^{-1}(j)) \notin E\}, \quad (13)$$

$$\mathcal{L}_{G,\sigma} = \{L \in \mathbb{R}^{d \times d} : L_{ii} = 1, L_{ij} = 0 \text{ for } i < j \text{ or } (\sigma^{-1}(i), \sigma^{-1}(j)) \notin E\}. \quad (14)$$

**Lemma 9** (Rose (1970); Paulsen et al. (1989)). *Let  $G = (V, E)$  be a chordal graph,  $\sigma$  an ordering of  $V$  which corresponds to a perfect elimination ordering of  $G$ . Then it holds that  $\Sigma \in \mathcal{S}_{G,\sigma}$  (13) if and only if  $L \in \mathcal{L}_{G,\sigma}$  (14), where  $L$  is the Cholesky factor of  $\Sigma$  such that  $\Sigma = LDL^T$ .*

Based on Lemma 9,  $G$  being chordal implies that, for a certain node permutation  $\sigma$  (corresponding to the permutation matrix  $P_\sigma$ ), the positive definite matrix  $\tilde{\Theta} := P_\sigma \Theta P_\sigma^\top$  belongs to  $\mathcal{S}_{G, \sigma_0}$  (13) and that the (lower-triangular) Cholesky factor matrix  $\tilde{L}$  of  $\tilde{\Theta}$  (such that  $\tilde{L}\tilde{D}\tilde{L}^\top = \tilde{\Theta}$  for a diagonal matrix  $\tilde{D}$ ) satisfies  $\tilde{L} \in \mathcal{L}_{G, \sigma_0}$  (14). As a consequence, the matrices  $(A, D)$  which are  $\sigma$ -similar to  $(\tilde{L}, \tilde{D})$ , i.e.,  $A := P_\sigma^\top \tilde{L} P_\sigma$  and  $D := P_\sigma^\top \tilde{D} P_\sigma$  satisfy:

$$ADA^\top = P_\sigma^\top \tilde{L} \tilde{D} \tilde{L}^\top P_\sigma = P_\sigma^\top \tilde{\Theta} P_\sigma = \Theta,$$

which means that  $A' = A\sqrt{D}$  satisfies  $A'A'^\top = \Theta$ . Moreover, it holds that  $E(A') \subset E(\Theta)$  because (i) the two support graphs are identical to  $E(\tilde{L})$  and  $E(\tilde{\Theta})$ , respectively, up to the node permutation  $\sigma$  and (ii)  $E(\tilde{L}) \subset E(\tilde{\Theta})$  by Lemma 9. Therefore  $A'A'^\top = \Theta$ . Note that  $A'$  is  $\sigma$ -similar to  $\tilde{L}D'$  (with diagonal  $D' = P_\sigma\sqrt{D}P_\sigma^\top$ ), which is a strict triangular matrix. Hence  $A'$  represents a DAG.  $\square$

## A.2 Proof of Proposition 5

*Proof.* The pair  $(B, \Omega)$  satisfies  $\varphi(B, \Omega) = \Theta$  by definition of the SEM given. It remains to prove that  $B$  also satisfies  $E(B) \subset E(\Theta_{\text{off}})$ . Indeed, note that Assumption 3 is equivalent to  $\Theta_{ij} \neq 0$  if  $(i, j) \in \mathcal{M}(B)$  (moralization of  $B$ ). Hence, in particular,  $\Theta_{i,j} \neq 0$  if  $B_{i,j} \neq 0$  or  $B_{j,i} \neq 0$ .  $\square$

## A.3 Proof of Theorem 6

*Proof.* The pair satisfying  $(B, \Omega^{\star-1}) \in \mathcal{S}(\Theta)$  entails that

$$(I - B)\Omega^{\star-1}(I - B)^\top = (I - B^*)\Omega^{\star-1}(I - B^*)^\top. \quad (15)$$

Now apply the following change of variable from  $B$  to  $\tilde{B}$ :

$$(I - B)\Omega^{\star-\frac{1}{2}} = \Omega^{\star-\frac{1}{2}}(I - \Omega^{\star\frac{1}{2}}B\Omega^{\star-\frac{1}{2}}) := \Omega^{\star-\frac{1}{2}}(I - \tilde{B}).$$

The same change of variable applies to  $B^*$  such that  $(I - B^*)\Omega^{\star-\frac{1}{2}} := \Omega^{\star-\frac{1}{2}}(I - \tilde{B}^*)$ . Then the equality (15) can be rewritten as  $\Omega^{\star-\frac{1}{2}}(I - \tilde{B})(I - \tilde{B})^\top \Omega^{\star-\frac{1}{2}} = \Omega^{\star-\frac{1}{2}}(I - \tilde{B}_0)(I - \tilde{B}_0)^\top \Omega^{\star-\frac{1}{2}}$ , i.e.,

$$(I - \tilde{B})(I - \tilde{B})^\top = (I - \tilde{B}^*)(I - \tilde{B}^*)^\top.$$

On the other hand,  $\tilde{B}^*$  and  $\tilde{B}$  are supported on DAGs, same as  $B^*$  and  $B$ , respectively, since they are the results of a diagonal scaling (by the diagonal matrix  $\Omega^{\star\frac{1}{2}}$  on the left and  $\Omega^{\star-\frac{1}{2}}$  on the right) applied on  $B^*$  and  $B$ , which preserves the support graph. Consequently, both  $(I - \tilde{B}^*)$  and  $(I - \tilde{B})$  are permutation similar to unit lower-triangular matrices (lower-triangular matrices with one's on the diagonal). The result then follows from (Loh and Bühlmann, 2014, Lemma 25), which confirms that if two square matrices  $X$  and  $Y$  are permutation similar to unit lower-triangular matrices such that  $XX^\top = YY^\top$ , then  $X = Y$ . Through this lemma,  $I - \tilde{B} = I - \tilde{B}^*$ , which concludes the proof.  $\square$



## A.4 Proof of Corollary 7

In the following proof, the technique using the diagonal information of  $\Theta$  in the EV case can be seen in, e.g., (Chen et al., 2019). The rest of the proof is based on Theorem 6 on one hand, and on the other hand, the theoretical framework of Ghassami et al. (2020) for proving *quasi-equivalence* between directed graphs from MLE-based causal discovery models. The notion of quasi-equivalence (Ghassami et al., 2020, Definition 9) is a generalization of Markov equivalence (between DAGs) for directed graphs.

Given a distribution  $\Theta$ , depending on the parametrization with respect to the causal graph  $G$ , a constraint on the entries of  $\Theta$  is called a *hard constraint* if the set of values satisfying that constraint is Lebesgue measure zero over the space of the parameters involved in the constraint. The set of hard constraints of a directed graph  $G$  is denoted by  $H(G)$ .

The two cited assumptions, needed for deducing quasi-equivalence between directed graphs, are restated as follows.

**Assumption** ((Ng et al., 2020, Assumptions 1–2)) *Under the same notations:*

(i) *A distribution  $\Theta$  is generalized faithful (g-faithful) to graph  $G$ , meaning that  $\Theta$  satisfies a hard constraint  $\kappa$  if and only if  $\kappa \in H(G)$ .*

(ii) *Let  $E(G)$  be the edge set of  $G$ . For a DAG  $G$  and a directed graph  $\hat{G}$ , it holds that*

- *$|E(\hat{G})| \leq |E(G)|$ , then  $H(\hat{G}) \not\subseteq H(G)$*
- *$|E(\hat{G})| < |E(G)|$ , then  $H(\hat{G}) \not\subseteq H(G)$*

*Proof.* (Corollary 7). First we prove two conditions before applying Theorem 6:

(i) Assumption 3 is satisfied under the generalized faithfulness assumption ((Ng et al., 2020, Assumption 1)). The distribution  $\Theta$  is such that  $\Theta = \varphi(B^*, \Omega^*)$  where  $B^*$  is supported on a DAG, denoted as  $G^*$ . Let  $i \in [d]$  and  $j \in [d], j \neq i$  be a pair such that  $\Theta_{ij} = 0$ , which is a hard constraint of  $\Theta$  denoted as  $\kappa$ . Then the g-faithfulness of  $\Theta$  entails that  $\kappa$  is also a hard constraint of the DAG  $G^*$ , i.e.,  $\kappa \in H(G^*)$ . Consequently, the nodes  $i$  and  $j$  must not be adjacent nor spouses in  $G^*$ . Because otherwise, the set of values taken by the parametrization (Lemma 1)

$$\Theta_{ij} = -\frac{B_{ij}^*}{\omega_j^{*2}} - \frac{B_{ji}^*}{\omega_i^{*2}} + \sum_{\ell=1}^d \frac{B_{i\ell}^* B_{j\ell}^*}{\omega_\ell^{*2}}$$

will have a nonzero Lebesgue measure, which contradicts with  $\kappa$  being a hard constraint of  $\Theta$ . Therefore,  $B^*$  (as an adjacency matrix of  $G^*$ ) must satisfy  $B_{ij}^* = B_{ji}^* = 0$  and  $B_{i\ell}^* B_{j\ell}^* = 0$  for all  $\ell$ , which yields Assumption 3.

(ii) It holds that  $D = \Omega^{*-1}$ , when the diagonal matrix  $D$  is defined by  $D_{ii} = \min_{j \in [d]} \{\Theta_{jj}\}$ ,  $\forall i \in [d]$ . This is because when the noise variances are equal, i.e.,  $\Omega_{ii}^* := \bar{\omega}^2 > 0$  for all  $i$ , then the diagonal terms of  $\Theta$ , from Lemma 1, are  $\Theta_{ii} = \frac{1}{\bar{\omega}^2} (1 + \sum_{\ell=1}^d B_{i\ell}^{*2})$ . Hence we have  $\min_{j \in [d]} \{\Theta_{jj}\} = \bar{\omega}^{-2}$ , which is attained because there is always a sink (a variable without child node) in the support DAG of  $B^*$ .

Now given  $D = \Omega^{\star-1}$ , let  $(B, D)$  be a solution to the  $\ell_0$  minimization problem (6). Then  $(B, D)$  necessarily belongs to the constrained set  $\mathcal{S}(\Theta)$  (4). Hence it follows from Theorem 6 that  $B = B^*$  as long as the support graph of  $B$  is a DAG. Therefore it remains to prove that  $B$  is acyclic. For this purpose, we evoke the proof of (Ng et al., 2020, Theorem 1) with necessary adaptations.

Denote the support graph of  $B$  as  $G$ . Since  $\Theta = \varphi(B, D)$ ,  $\Theta$  contains all distributional constraints of  $G$ . Hence  $H(G) \subset H(G^*)$  under the g-faithfulness assumption. On the other hand, the solution  $B$  is such that  $\|B\|_{\ell_0}$  is minimal among all feasible elements in  $\mathcal{S}(\Theta)$  including  $B^*$ , hence  $|E(G)| \leq |E(G^*)|$ . By (Ng et al., 2020, Assumption 2) we have  $H(G) \not\subset H(G^*)$ . Therefore it holds that  $H(G) = H(G^*)$ , and  $G$  is quasi equivalent to  $G^*$ .

Finally, suppose by contraction that  $G$  has cycles. Let  $C = (X_1, \dots, X_c, X_1)$  be a smallest (shortest) cycle on  $G$ . By quasi equivalence,  $G^*$  and  $G$  should have the same adjacencies (either via a real edge or a virtual edge (Richardson, 1996)),  $B^*$  should also have nonzeros in the location of all the edges of  $C$ .

- If  $|C| > 3$ , then the DAG  $G^*$  has a v-structure, denoted as  $(\mathbf{X}_{i-1} \rightarrow \mathbf{X}_i \leftarrow \mathbf{X}_{i+1})$ , which entails the existence of a subset of nodes  $S$ ,  $\mathbf{X}_i \notin S$ , such that  $\mathbf{X}_{i-1} \perp\!\!\!\perp \mathbf{X}_{i+1} | S$ . However this conditional independence relation is not true for  $G$  (given the cycle). This contradicts with quasi equivalence.
- If  $|C| = 3$ , then  $G$  should also have a triangle on the same triplet of nodes, which contradicts the triangle condition.
- If  $|C| = 2$ . Let  $C = (X_1, X_2, X_1)$ . If none of the adjacencies in  $G$  to  $C$  are in-going, then  $C$  can be reduced to a single edge and the resulting directed graph is equivalent to  $G$  (Ghassami et al., 2020). Hence, due to the edge number minimality, such  $C$  is not possible. If there exists an in-going edge, say from  $X_p$  to one end of  $C$ , there will be a virtual or real edge to the other end of  $C$  as well. Therefore,  $X_p$ ,  $X_1$ , and  $X_2$  are adjacent in  $G$  and hence in  $G^*$ , which contradicts the triangle condition. Also, if the edge between  $X_p$  and one end of  $C$  is a virtual edge,  $X_p$  should have a real edge towards another cycle in  $G$ , which, with the virtual edge, again forms a triangle, and hence contradicts the triangle condition.

In conclusion, in all cases, quasi equivalence or the triangle assumption is violated, which is a contradiction. Therefore the support graph of  $B$  is a DAG.  $\square$

## B Algorithms and computational details

For a diagonal matrix  $D \succ 0$ , the smooth part of the augmented Lagrangian of ICID (7) or (8) at  $(B, \Lambda) \in \mathbb{R}^{d \times d} \times \mathbb{R}^{d \times d}$ , denoted as  $\tilde{L}^\rho(B, \Lambda)$ , is

$$\tilde{L}^\rho(B, \Lambda) = r(B) + \langle \Lambda, \Theta - \varphi_D(B) \rangle + \frac{\rho}{2} \|\Theta - \varphi_D(B)\|_F^2 \quad (16)$$

where  $\varphi_D(B) := (I - B)D(I - B)^T$  and  $r(B)$  is either zero or the regularization function of (8).

The function (16) is linear in  $\Lambda$ , and the gradient  $\nabla_{\Lambda} \tilde{L}^{\rho}(B, \Lambda) = \Theta - \varphi_D(B)$  is used in the dual ascent step in Algorithm 1. The gradient and Hessian of  $\tilde{L}^{\rho}(\cdot, \Lambda)$  in  $B$  are given in the following proposition.

**Proposition 10.** *For a diagonal  $D \succ 0$  and  $\Lambda \in \mathbb{R}^{d \times d}$ , the gradient and Hessian of  $\tilde{L}^{\rho}(\cdot, \Lambda)$  (16) are as follows:*

$$\begin{aligned} \nabla_B \tilde{L}^{\rho}(B, \Lambda) &= 2(\Lambda + \rho(\Theta - \varphi_D(B)))(I - B)D + \nabla_{Br}(B) \\ \nabla_B^2 \tilde{L}^{\rho}(B, \Lambda)[Z] &= 2\left(4\rho \cdot \text{Sym}(ZD(I - B)^{\text{T}})(I - B)D - (\Lambda + \rho(\Theta - \varphi_D(B)))ZD\right) + \nabla_B^2 r(B)[Z] \end{aligned}$$

where  $\text{Sym}(X) := \frac{X+X^{\text{T}}}{2}$ . When  $r(B)$  is nonzero, for  $r(B) := \lambda_2 \text{tr}(\tilde{M}^{\text{T}}(B \odot B))$  in (8), we have

$$\nabla_{Br}(B) = 2\lambda_2 \tilde{M} \odot B, \quad \text{and} \quad \nabla_B^2 r(B)[Z] = 2\lambda_2 \tilde{M} \odot Z. \quad (17)$$

*Proof.* The gradient and Hessian (17) of the regularizer  $r(B)$ , in the case of the regularized ICID (8), can be obtained from straightforward calculus. Next, by setting the regularization back to zero, we denote the remaining part of (16) as  $\tilde{L}^{\rho}(\cdot, \Lambda)$ . The differential of  $\varphi_D(\cdot)$  in (16) is as follows,

$$D\varphi_D(B)[Z] = -2 \cdot \text{Sym}(ZD(I - B)^{\text{T}}) \quad (18)$$

for any  $Z \in \mathbb{R}^{d \times d}$ . It follows that

$$\langle \nabla_B \tilde{L}^{\rho}(B, \Lambda), Z \rangle = 2 \left\langle \underbrace{\Lambda + \rho(\Theta - \varphi_D(B))}_{\phi_1(B)}, \underbrace{\text{Sym}(ZD(I - B)^{\text{T}})}_{\phi_2(B)} \right\rangle. \quad (19)$$

This entails that

$$\nabla_B \tilde{L}^{\rho}(B, \Lambda) = 2(\Lambda + \rho(\Theta - \varphi_D(B)))(I - B)D.$$

For the Hessian: the differentials of  $\phi_1(B)$  and  $\phi_2(B)$  in (19) are:

$$D\phi_1(B)[Z] = 2\rho \text{Sym}(ZD(I - B)^{\text{T}}) \quad \text{and} \quad D\phi_2(B)[Z] = -ZDZ^{\text{T}}.$$

Hence, by differentiating the right-hand side of (19), we have

$$\langle Z, \nabla_B^2 \tilde{L}^{\rho}(B, \Lambda)[Z] \rangle = 2 \left( \underbrace{2\rho \|\text{Sym}(ZD(I - B)^{\text{T}})\|_{\text{F}}^2}_{a_1(B)} - \underbrace{\langle \Lambda + \rho(\Theta - \varphi_D(B)), ZDZ^{\text{T}} \rangle}_{a_2(B)} \right). \quad (20)$$

The first term  $a_1(B)$  on the right-hand side is

$$\begin{aligned} a_1(B) &= 2\rho \left( \text{tr}((I - B)DZ^{\text{T}}\text{Sym}(ZD(I - B)^{\text{T}})) + \text{tr}(ZD(I - B)^{\text{T}}\text{Sym}(ZD(I - B)^{\text{T}})) \right) \\ &= 2\rho \left( \text{tr}(Z^{\text{T}}\text{Sym}(ZD(I - B)^{\text{T}})(I - B)D) + \text{tr}(D(I - B)^{\text{T}}\text{Sym}(ZD(I - B)^{\text{T}})Z) \right) \\ &= 4\rho \text{tr} \left( Z^{\text{T}}\text{Sym}(ZD(I - B)^{\text{T}})(I - B)D \right), \end{aligned}$$

and  $a_2(B)$  is

$$a_2(B) = \text{tr} \left( ZDZ^T(\Lambda + \rho(\Theta - \varphi_D(B))) \right) = \text{tr} \left( Z^T(\Lambda + \rho(\Theta - \varphi_D(B)))ZD \right).$$

Through (20) we have

$$\nabla_B^2 \tilde{L}^\rho(B, \Lambda)[Z] = 2 \left( 4\rho \cdot \text{Sym}(ZD(I - B)^T)(I - B)D - (\Lambda + \rho(\Theta - \varphi_D(B)))ZD \right).$$

□

## B.1 Primal problem solver for ICID

The FISTA (Beck and Teboulle, 2009) is used for solving (11) in view of the  $\ell_1$ -norm term. The adaptation of FISTA is detailed in Algorithm 2.

---

**Algorithm 2** FISTA for the primal problem (11) of ICID

---

**Input:** Inverse covariance matrix  $\Theta \in \mathbb{R}^{d \times d}$ , objective function  $F(\cdot) := \tilde{L}^\rho(\cdot, \Lambda)$  of (11),

$\alpha_0 > 0$ ,  $\gamma \in (0, 1)$ ,  $\beta = \frac{1}{2}$ , tolerance  $\epsilon$

1: Initialize:  $B_0 = \mathbf{0}_{d \times d}$ , set  $Y_0 = W_0$ .

2: **for**  $s = 1, 2, \dots$  **do**

3: Backtracking: find smallest integer  $k_s \geq 0$  such that, for  $\eta_s := \alpha_0 \beta^{k_s}$ , # see (26)

$$F(\tilde{B}) - F(Y_{s-1}) \leq -\gamma \eta_s \|\text{grad}_{E_\Theta} F(Y_{s-1})\|^2,$$

where

$$\tilde{B} = \text{prox}_{\eta_s \ell_1} \left( Y_{s-1} - \eta_s \text{grad}_{E_\Theta} F(Y_{s-1}) \right).$$

# see (22)-(23)

4: Update FISTA iterates:

$$B_s = \tilde{B} \quad \text{and} \quad Y_s = B_s + \frac{s-1}{s+2} (B_s - B_{s-1}).$$

5: Stop if  $\|\Delta(B_s)\|_F \leq \epsilon$ :  
return  $B_s$

# see (24)

6: **end for**

---

**Support constraint of ICID.** The support constraint of ICID is entirely reflected in the primal problem (11) in the form of  $B \in E_\Theta$  where  $E_\Theta$  (5), i.e.,

$$E_\Theta = \{B \in \mathbb{R}^{d \times d} : B_{ij} = 0 \quad \forall i = j \text{ or } (i, j) \notin \mathbf{E}(\Theta)\} \quad (21)$$

is a linear subspace of  $\mathbb{R}^{d \times d}$  with dimension  $(\|\Theta\|_0 - d)$ . Hence the support constraint of (11) can be satisfied using subspace projection, which has the following form.

**Definition 11.** Given (an adjacency matrix)  $S \in \mathbb{R}^{d \times d}$ , the projection onto the support graph  $E(S)$  is denoted and defined as  $P_S : \mathbb{R}^{d \times d} \rightarrow \mathbb{R}^{d \times d}$  such that

$$(P_S(Z))_{ij} = \begin{cases} Z_{ij} & \text{if } (i, j) \in E(S) \\ 0 & \text{otherwise.} \end{cases}$$

It follows that the gradient of  $\tilde{L}^\rho(\cdot, \Lambda)$  restricted to subspace  $E_\Theta$ , denoted as  $\text{grad}_{E_\Theta} F(\cdot)$ , is

$$\text{grad}_{E_\Theta} F(B) = P_{E_\Theta}(\nabla_B \tilde{L}^\rho(B, \Lambda)) \quad (22)$$

where  $\nabla_B \tilde{L}^\rho(B, \Lambda)$  is computed in Proposition 10 and  $P_{E_\Theta}$  is given in Definition 11.

On the other hand, the proximal operator associated with the  $\ell_1$  term of (11) is

$$\text{prox}_{\lambda \ell_1}(Z) = \begin{cases} \text{sign}(Z_{ij})(|Z_{ij}| - \eta) & \text{if } |Z_{ij}| \geq \lambda \\ 0 & \text{otherwise.} \end{cases} \quad (23)$$

**Stopping criterion.** In Algorithm 2, line 5, the stopping criterion at each iteration (with a given  $\Lambda \in \mathbb{R}^{d \times d}$ ) is defined with respect to the optimality of the primal problem (11). For clarity, we rewrite the smooth and non-smooth parts of the augmented Lagrangian as follows,

$$g(x) := \|x\|_{\ell_1} \quad \text{and} \quad \tilde{L}^\rho(x, y) := \tilde{L}^\rho(B, \Lambda)$$

for  $x := \text{vec}(B)$  and  $y := \text{vec}(\Lambda)$ .

Then, an iterate  $x$  is optimal if  $-\nabla_x \tilde{L}^\rho(x, y) \in \partial g(x)$ . This set-valued criterion can be further expressed as the following distance, for  $u := -\nabla_x \tilde{L}^\rho(x, y)$ ,

$$\Delta(B) := \text{dist}(u, \partial g(x)) = \|(I - P_{\partial g(x)})(u)\| \leq \epsilon, \quad (24)$$

where the projection term  $P_{\partial g(x)}(u)$  can be obtained through the closed-form expression of  $\partial g(x)$  (Cartesian product of  $\partial|x_i|$  along each of the  $d^2$  dimensions). Hence the expression of  $\Delta(B)$  in (24) is: for  $i = 1, \dots, d^2$ ,

$$((I - P_{\partial g(x)})(u))_i = \begin{cases} 1 + u_i & \text{if } (x_i < 0) \vee ((x_i = 0) \wedge (u_i < -1)) \\ 0 & \text{if } (x_i = 0) \wedge (|u_i| \leq 1) \\ -1 + u_i & \text{if } (x_i > 0) \vee ((x_i = 0) \wedge (u_i > 1)). \end{cases} \quad (25)$$

**Selection of initial stepsizes.** We adapt the initial stepsize  $\alpha_0$  in Algorithm 2 at each iteration through the quadratic approximation of the exact line search objective. More precisely, given a descent direction  $Z$ , we define  $\alpha_0$  as the minimizer of the following quadratic approximation of  $\tilde{L}^\rho(B + \alpha Z, \Lambda)$  along  $Z$ ,

$$\alpha_0 := \min_{\alpha > 0} \alpha \langle \nabla_B \tilde{L}^\rho(B, \Lambda), Z \rangle + \alpha^2 \langle Z, \nabla_B^2 \tilde{L}^\rho(B, \Lambda)[Z] \rangle, \quad (26)$$

which gives

$$\alpha_0 := -\frac{\langle \nabla_B \tilde{L}^\rho(B, \Lambda), Z \rangle}{2 \langle Z, \nabla_B^2 \tilde{L}^\rho(B, \Lambda)[Z] \rangle},$$

where the two terms on the right-hand side are given in (19) and (20) respectively; see proof of Proposition 10. In the experiments, the computation rule of  $\alpha_0$  (26) is applied during the first 10 FISTA iterations (Algorithm 2, line 3) and then the value of  $\alpha_0$  is fixed at its latest value. The other line search parameters in Algorithm 2 are:  $\gamma = \frac{1}{2}$ , and maximal number of backtrackings  $\bar{n}_{ls} = 20$ .

*Remark 12* (Computational cost). The computation of  $\nabla_B \tilde{L}^\rho(B, \Lambda)$  (Proposition 10) costs  $O(kd^2)$  floating-point operations, where  $k$  is the maximal node degree of  $\Theta$ , which equals the maximal Markov blanket size of  $B$  under Assumption 3.

### Parameter values.

- For Algorithm 2: The tolerance parameter is set as  $\epsilon = 10^{-4}$ . The maximal number of FISTA iterations is set as 3000 for the experiments of Section 4.3, and 1000 for the experiments of Section 4.2.
- For Algorithm 1: The tolerance parameter of the global ALM is set as  $\epsilon = 5 \cdot 10^{-3}$ . The maximal number of ALM iterations is set to 3, which turns out to be empirically sufficient in the experiments of Section 4.3. In the experiments of Section 4.2, the maximal number of ALM iterations is set as 3 for  $\mathcal{O}$ -ICID and as 1 for ICID (in Section 4.2). In the experiments of Section 4.4, the maximal number of ALM iterations is set as 4.

The initial value of  $\rho$  (for the augmented Lagrangian function) is  $\rho := 1$ . In Algorithm 1, line 3, if the relative decrease in the residual  $\|\Theta - \varphi_D(B)\|$  is weaker than 0.05, then a new primal descent attempt will start after incrementing the value of  $\rho$  by  $\rho \leftarrow 1.2 \cdot \rho$ .

## B.2 ICID followed by DAG projection

Algorithm 3 shows a combination of ICID with a method for computing proximal DAGs. The exponential trace function  $h(\cdot)$  in NOTEARS Zheng et al. (2018) is used in the proximal DAG computation.

In this algorithm, the proximal mapping (28) is defined as a solution to

$$\min_{B \in \mathbb{R}^{d \times d}} h(B) + \frac{1}{\gamma_2} \underbrace{\|B - c_0 B_{t+1}\|_F^2}_{g(B; B_{t+1})}, \quad (29)$$

where  $h$  is the exponential trace-based function

$$h(B) = \text{tr}(\exp(|B|))$$

with the absolute value operation  $|\cdot|$  applied to  $B$  element-wisely.

---

**Algorithm 3** DAG-constrained ICID

---

**Input:** Observational data  $X \in \mathbb{R}^{d \times n}$

- 1: Get  $\Theta$  from Inverse covariance estimator (Algorithm 4)
- 2: Compute  $B_0$  by ICID (Algorithm 1)
- 3: **for**  $t = 1, \dots$ , **do**
- 4:   **if** stopping criteria( $B_t, \tilde{B}_t$ ) attained **then**
- 5:     return  $B_t$
- 6:   **end if**
- 7:   Compute proximal mappings:

$$B_{t+1} = (1 - \rho)B_0 + \rho\tilde{B}_t \tag{27}$$

$$\tilde{B}_{t+1} = \text{prox}_{\gamma_2 h}(c_0 B_{t+1}) \tag{28}$$

- 8:   Increment  $\gamma_2$
  - 9: **end for**
- 

Due to the exponential trace in  $h$  (Zheng et al., 2018), problem (29) is nonconvex. We resort to the search of one proximal point (28) satisfying sufficient decrease in  $h$ . In view of reducing the cost for computing the gradients of the exponential trace function  $h$  in (28), the low-rank method LoRAM-AGD of Dong and Sebag (2022) is used. The increment rule line 8 is an ad-hoc adaptation of the AMA (alternating minimization algorithm) for optimizing the Lagrangian of an equality constrained optimization. In the experiment on large graphs, the computation of ICID (line 2) is limited to one single ALM iteration.

### B.3 An empirical inverse covariance estimator

In the experiments, we use a basic empirical inverse covariance estimator for construction input matrices of ICID and GH18.

In the computation of (30), the pseudo-inverse coincides with the inverse of  $\hat{C}$  when  $\hat{C}$  is positive definite (e.g., when the number  $n$  of samples is sufficiently large). In (31), the subscript ‘off’ indicates the following filtering operation

$$\Theta_{\text{off}} = \{\Theta_{ij} : i \neq j\}$$

where the indices of the remaining (off-diagonal) entries are preserved.

**Selection of  $\lambda_1$  for Algorithm 4.** In the experiment for Figure 1, a parameter selection is needed. We use grid search for selecting values of  $\lambda_1$  for the empirical inverse covariance estimator (Algorithm 4). Note that the total time for selecting the value of  $\lambda_1$  using Algorithm 4 is included in the computation time of ICID in the benchmark of Figure 1.

We start by estimating the grid search area of  $\lambda_1$ , based on observational data on ER graphs with  $200 \leq d \leq 2.10^3$  nodes. The same methodology applies to SF graphs.

---

**Algorithm 4** Empirical inverse covariance estimator
 

---

**Input:** Data matrix  $X \in \mathbb{R}^{n \times d}$ , parameter  $\lambda_1 \in (0, 1)$

**Output:**  $\hat{\Theta}_{\lambda_1} \in \mathbb{R}^{d \times d}$

- 1: Compute empirical covariance and its inverse:

$$\hat{C} = \frac{1}{n}(X - \bar{X})^T(X - \bar{X}) \quad \text{and} \quad \hat{\Theta} = \hat{C}^\dagger, \quad (30)$$

where  $\hat{C}^\dagger$  denotes the pseudo-inverse of  $\hat{C}$ .

- 2: Element-wise thresholding on off-diagonal entries:

$$\begin{aligned} \text{diag}(\hat{\Theta}_{\lambda_1}) &:= \text{diag}(\hat{\Theta}), \\ (\hat{\Theta}_{\lambda_1})_{\text{off}} &:= \mathbb{H}(\hat{\Theta}_{\text{off}}, \lambda_1 \|\hat{\Theta}_{\text{off}}\|_{\max}), \end{aligned} \quad (31)$$

where  $\mathbb{H}$  is defined as

$$\mathbb{H}(y, \tau) = \begin{cases} y & \text{if } |y| \geq \tau \\ 0 & \text{otherwise.} \end{cases}$$


---

Given that most desired causal structures have an average degree  $1 \leq \text{deg} \leq 4$ , the target sparsity of  $\hat{\Theta}_{\lambda_1}$  by Algorithm 4 is bounded by  $\bar{\rho}_{\text{deg}} = \max(\frac{\text{deg}}{d}) \approx 2.0\%$  for graphs with  $d \geq 200$  nodes. This gives us an approximate target percentile of around 98%, i.e., top 2% edges in terms of absolute weight of  $\hat{\Theta}_{\text{off}}$ . In other words, the maximal value  $\lambda_1^{\max}$  of the grid search area is set as  $\lambda_1^{\max} := \frac{|\hat{\Theta}_{\text{off}}(\tau_{98})|}{\|\hat{\Theta}_{\text{off}}\|_{\max}}$ , where  $\tau_{98}$  refers to the index of the 98-th percentile in  $\{|\hat{\Theta}_{\text{off}}|\}$ . For the experiments with ER2 graphs in Section 4, the estimated  $\lambda_1^{\max}$  is  $6.10^{-1}$ . Hence, the search grid of  $\lambda_1$  is set up as  $n_{I_1} = 20$  equidistant values on  $I_1 = [10^{-2}, 6.10^{-1}]$ .

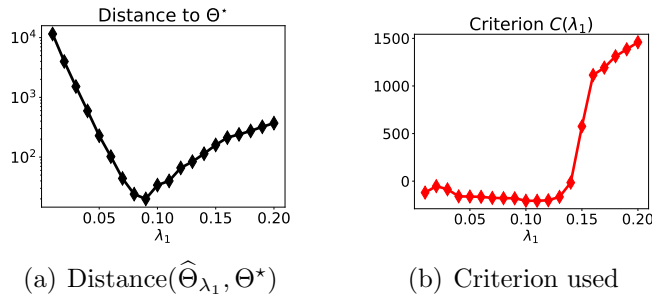


Figure 4: Grid search of  $\lambda_1$  with Algorithm 4 based on criterion  $C(\lambda_1)$  (32). Data  $X$  is from linear SEM with Gaussian noise, on ER2 graph with  $d = 200$  nodes.

The selection criterion, similar to GraphicalLasso, is defined as

$$C(\lambda_1) := \text{tr}(\hat{C}\hat{\Theta}_{\lambda_1}) - \log \det(\tilde{\Theta}_{\lambda_1}), \quad (32)$$



where  $\tilde{\Theta}_{\lambda_1} = \hat{\Theta}_{\lambda_1} + \frac{9}{10} \text{diag}(\hat{\Theta}_{\lambda_1})$  is used in the log det-evaluation for an enhanced positive definiteness in all cases.

Figure 4 shows the criterion values compared to the Hamming distances with the oracle precision matrix  $\Theta^* := \phi(B^*)$ . We observe that the selection criterion with  $\arg \min_{I_1} C(\lambda_1)$  gives an answer that is rather close to the optimal value in terms of distance of  $\hat{\Theta}_{\lambda_1}$  to the oracle precision matrix  $\Theta^*$ .

## B.4 The skewness-based regularization

The matrix  $\tilde{M}$  in the regularized ICID (8), based on third-order cumulant statistics (Hyvärinen and Smith, 2013, Eq. (18)), is the negative of the following matrix:

$$M = C \odot \mathbb{E}[\mathbf{X}g(\mathbf{X})^T - g(\mathbf{X})\mathbf{X}^T] \quad (33)$$

where  $C$  denotes the correlation matrix of  $\mathbf{X}$  and  $g(\cdot)$  applies to  $\mathbf{X}$  elementwisely.

**Effect of skewness on the matrix  $M$ .** Suppose that the pairwise model between  $x := X_i$  and  $y := X_j$  is  $y = \rho x + u$  if  $x \rightarrow y$  and is  $x = \rho y + u$  if  $y \rightarrow x$ , where  $|\rho| < 1$ . The third-order cumulant-based statistic (Hyvärinen and Smith, 2013, Eq. (10)) is defined as follows:

$$\tilde{R}_{c3}(x, y) := \rho \mathbb{E}[x^2 y - x y^2]. \quad (34)$$

Then the  $(i, j)$ -th term of  $M$  is

$$M_{ij} = C_{ij} \mathbb{E}[X_i^2 X_j - X_i X_j^2] = \frac{1}{\rho} C_{ij} \tilde{R}_{c3}(x, y)$$

which is positive if  $X_i \rightarrow X_j$  and otherwise is negative.

On the other hand, the following theorem shows the connection between  $\tilde{R}_{c3}$  and the causal parameter  $\rho$  depending on the skewness:

**Theorem 13** ((Hyvärinen and Smith, 2013, Theorem 2)). *If the causal direction is  $x \rightarrow y$ , then*

$$\tilde{R}_{c3} = \text{skew}(x)(\rho^2 - \rho^3)$$

*and if the causal direction is the opposite, then*

$$\tilde{R}_{c3} = \text{skew}(y)(\rho^3 - \rho^2).$$

Therefore, when the variables of  $\mathbf{X}$  are positively skewed, we obtain the following table about the signs of  $M_{ij}$  and signs of  $\rho$ .

Table 2: Signs of  $M_{ij}$  for different signs of  $\rho$  and different pairwise causal directions.

Direction	$\rho( \rho  < 1)$	$C_{ij}$	$\tilde{R}_{3c}$	$M_{ij}$
$x \rightarrow y$	$> 0$	+	+	+
$x \rightarrow y$	$< 0$	-	+	+
$x \leftarrow y$	$> 0$	+	-	-
$x \leftarrow y$	$< 0$	-	-	-

As the table above suggests, the sign of  $M_{ij}$  is mostly positive if the causal direction is  $(X_i \rightarrow X_j)$  and otherwise it is negative.

This motivates us to define the regularization term of the regularized ICID (8) as

$$r(B) := \text{tr}(\tilde{M}^T(B \odot B)).$$

Since with positive skewness, the trace value  $r(B)$  is small (possibly negative) when the pairwise causal directions in  $B$  are consistent with the signs of the pairwise measures encoded in  $M = -\tilde{M}$ , and is large when the pairwise directions in  $B$  are reversed.

## B.5 Parameter selection for ICID and ICID (skew)

We optimize ICID (skew), the regularized ICID (8), using the same algorithm (Algorithm 1) as ICID. Computationally, ICID (skew) differs with ICID only in the additional regularization function  $r(B)$ , which is subsumed in the proposed FISTA subroutine (Algorithm 2) according to Proposition 10.

Both ICID and ICID (skew) uses as input the estimated inverse covariance matrix by Algorithm 4, which has a selection rule for the parameter  $\lambda_1$  given a set values; see Appendix B.3. In the experiment on sythetic data, the set for selection is composed of the 10 linearly equal distant values  $\lambda_1 \in [0.04, 0.1]$ . In the experiment on the fMRI datasets, the set for selection is 10 linearly equal distant values of  $\lambda_1 \in [0.01, 0.1]$ .

Subsequently, both ICID and ICID (skew) are optimized by Algorithm 1 for a parameter  $\rho > 0$ , which determines the initial weight of the  $\ell_1$  term in the augmented Lagrangian. In practice, we used a small set of values  $\lambda'_1 := \frac{1}{\rho} \in \{0.05, 0.1, 0.2, 0.3\}$  for the experiments on synthetic data (Section 4.2), and  $\lambda'_1 := \frac{1}{\rho} \in \{0.01, 0.05, 0.06, 0.07, 0.08, 0.1, 0.2\}$  for the experiments on the fMRI datasets.

The one additional regularization parameter  $\lambda_2$  for ICID (skew) is also selected by a simple grid search, given a fixed pair of preselected parameters  $(\lambda_1, \rho)$  of ICID. The grid search result for  $\lambda_2$  on the fMRI Sim4 data is as follows:

Table 3: Grid search for the regularization parameter  $\lambda_2$  of ICID (skew).  $\lambda_1$  is the parameter for sparse inverse covariance estimation (Algorithm 4) and  $\lambda'_1 := 1/\rho$  is the ALM parameter in Algorithm 1.

<i>fMRI Sim4</i>	$(\lambda_1, \lambda'_1, \lambda_2)$	SHD	TPR	FDR	nnz	Primal optimality
ICID	(0.0256, 0.05, 0.00)	14	0.820	0.219	64	1.1e-5
ICID (skew)	(0.0256, 0.05, 0.01)	18	0.787	0.273	66	2.1e-5
ICID (skew)	(0.0256, 0.05, 0.02)	12	0.934	0.173	69	6.2e-5
ICID (skew)	(0.0256, 0.05, 0.03)	7	0.967	0.106	66	2.3e-5
ICID (skew)	(0.0256, 0.05, 0.05)	5	0.984	0.076	65	9.2e-5
ICID (skew)	(0.0256, 0.05, 0.09)	6	0.984	0.090	66	5.0e-6

The learning accuracy of the estimated graphs during the grid search are visualized in the following ROC curves.

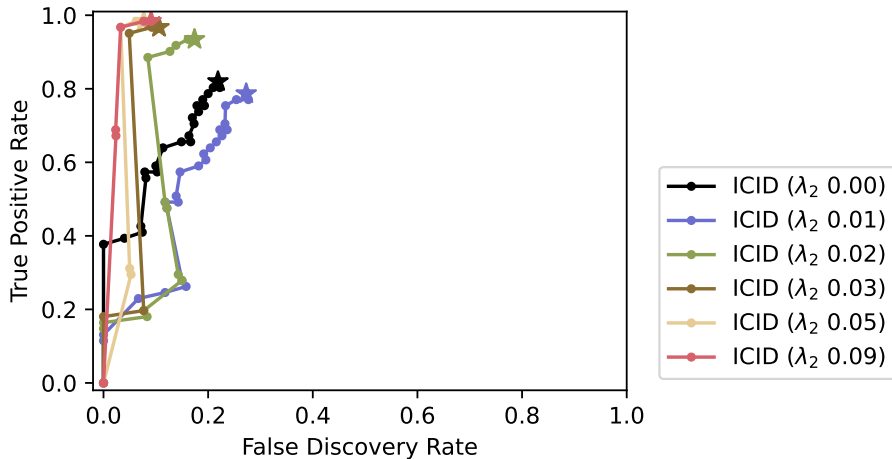


Figure 5: ROC curves of ICID (skew) with different values of  $\lambda_2$  on the fMRI Sim4 dataset.. The x-axis is the FDR scores instead of FPRs.

## C Experiments

The codes of the proposed algorithms are available at <https://anonymous.4open.science/r/icid-v2-9611>.

### C.1 Random graphs and synthetic data

The experiments on synthetic data are conducted with DAGs generated from two sets of random graphs: (i) Erdős–Rényi (ER) graphs and (ii) Scale-free (SF) (Barabási and Albert, 1999) graphs, as characterized in Table 4.

Table 4: Features of different graph models.

	Parameter	Degree distribution
Erdős-Rényi	$p \in (0, 1)$	Binomial $\mathcal{B}(d, p)$
Scale-free	$\gamma$	$P(k) \propto k^{-\gamma}$

The generation of random DAGs from the two sets above is the same as in (Zheng et al., 2018). The naming of these graphs has a node degree specification, such as ‘ER1’, where the number indicates the average node degree of the graph. Specifically, for a given DAG  $G^*$ , its weighted adjacency matrix  $B^*$  is generated by assigning weights to the nonzeros of  $\mathbb{B}(G^*) \in \{0, 1\}^{d \times d}$  independently from the uniform distribution:  $B_{ij}^* \sim \text{Unif}([-2, -0.5] \cup [0.5, 2])$ , for  $(i, j) \in E(\mathbb{B}(G^*))$ . We generate observational data according to the linear SEM model (2), and store them in dataset  $X \in \mathbb{R}^{n \times d}$  where  $n$  is the number of samples. The additive noises of the linear SEM such that  $X = B^{*\top} X + E$ , belong to either of the following models: (i) Gaussian noise (Gaussian):  $E \sim \mathcal{N}(0, \Omega)$  and (ii) Exponential noise (Exponential):  $E \sim \text{Exp}(\Omega)$ , where  $\Omega$  is a diagonal matrix of

noise variances. Therefore, the dataset  $X$  belongs to one of the following categories  $\{\text{ER deg, SF deg}\} \times \{\text{Gaussian, Exponential}\}$  (where deg is the aforementioned average node degree).

## C.2 Evaluation Metrics

The graph metrics for the comparison of graph edge sets are the commonly used (e.g., by the aforementioned baseline methods) ones as follows:

- (1)  $\text{TPR} = \text{TP}/\text{T}$  (higher is better),
- (2)  $\text{FDR} = (\text{R} + \text{FP})/\text{P}$  (lower is better),
- (3)  $\text{FPR} = (\text{R} + \text{FP})/\text{F}$  (lower is better),
- (4)  $\text{SHD} = \text{E} + \text{M} + \text{R}$  (lower is better).

More precisely, SHD is the (minimal) total number of edge additions (E), deletions (M), and reversals (R) needed to convert an estimated DAG into a true DAG. Since a pair of directed graphs are compared, a distinction between True Positives (TP) and Reversed edges (R) is needed: the former is estimated with correct direction whereas the latter is not. Likewise, a False Positive (FP) is an edge that is not in the undirected skeleton of the true graph. In addition, Positive (P) is the set of estimated edges, True (T) is the set of true edges, False (F) is the set of non-edges in the ground truth graph. Finally, let (E) be the extra edges from the skeleton, (M) be the missing edges from the skeleton.

## C.3 Causal structure learning from inverse covariance matrices

The results of the experiment in Section 4.3 are also represented in Table 5 and Table 6.

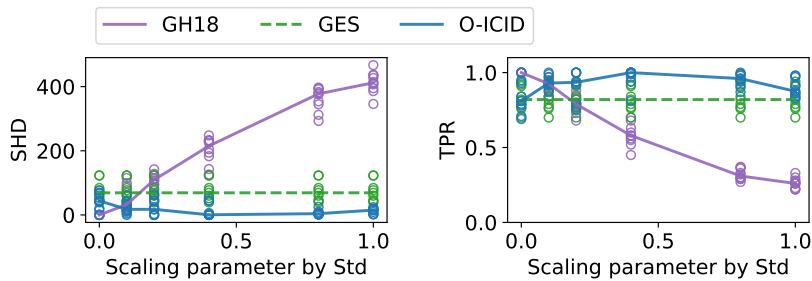
Table 5: Results of causal structure learning from inverse covariance matrices in the EV case ( $\lambda = 0$ ) and the NV cases ( $\lambda > 0$ ). The scaling parameter  $\lambda$  is defined in (12).

G	$\lambda$	Algorithm	TPR	SHD	Median SHD	time (seconds)
ER1	0.00	GH18	$1.000 \pm 0.000$	$0.000 \pm 0.000$	0.000	$0.006 \pm 0.003$
		GES	$0.894 \pm 0.053$	$31.700 \pm 7.103$	29.000	$386.155 \pm 56.533$
		$\mathcal{O}$ -ICID	$0.922 \pm 0.057$	$9.800 \pm 5.350$	10.500	$1.616 \pm 0.771$
	0.10	GH18	$0.976 \pm 0.026$	$3.500 \pm 4.378$	2.000	$0.006 \pm 0.003$
		GES	$0.894 \pm 0.053$	$31.700 \pm 7.103$	29.000	$269.355 \pm 80.731$
		$\mathcal{O}$ -ICID	$0.958 \pm 0.047$	$4.900 \pm 5.446$	4.000	$1.336 \pm 0.431$
	0.20	GH18	$0.896 \pm 0.071$	$13.900 \pm 9.433$	11.500	$0.005 \pm 0.006$
		GES	$0.894 \pm 0.053$	$31.700 \pm 7.103$	29.000	$223.234 \pm 65.922$
		$\mathcal{O}$ -ICID	$0.970 \pm 0.057$	$2.900 \pm 5.953$	0.000	$1.321 \pm 0.345$
	0.40	GH18	$0.736 \pm 0.082$	$36.000 \pm 13.174$	33.000	$0.004 \pm 0.001$
		GES	$0.894 \pm 0.053$	$31.700 \pm 7.103$	29.000	$202.746 \pm 44.534$
		$\mathcal{O}$ -ICID	$0.996 \pm 0.013$	$0.500 \pm 1.581$	0.000	$1.741 \pm 0.243$
	0.80	GH18	$0.514 \pm 0.071$	$65.500 \pm 12.457$	62.500	$0.004 \pm 0.001$
		GES	$0.894 \pm 0.053$	$31.700 \pm 7.103$	29.000	$183.254 \pm 28.068$
		$\mathcal{O}$ -ICID	$1.000 \pm 0.000$	$0.000 \pm 0.000$	0.000	$1.452 \pm 0.424$
	1.00	GH18	$0.414 \pm 0.087$	$82.600 \pm 17.424$	81.500	$0.005 \pm 0.003$
		GES	$0.894 \pm 0.053$	$31.700 \pm 7.103$	29.000	$181.916 \pm 28.672$
		$\mathcal{O}$ -ICID	$0.992 \pm 0.017$	$0.400 \pm 0.843$	0.000	$1.251 \pm 0.282$
ER2	0.00	GH18	$1.000 \pm 0.000$	$0.000 \pm 0.000$	0.000	$0.004 \pm 0.000$
		GES	$0.828 \pm 0.082$	$73.889 \pm 31.700$	69.000	$1076.755 \pm 1063.638$
		$\mathcal{O}$ -ICID	$0.827 \pm 0.113$	$43.700 \pm 23.443$	44.000	$1.651 \pm 0.860$
	0.10	GH18	$0.912 \pm 0.044$	$49.700 \pm 36.999$	32.500	$0.004 \pm 0.000$
		GES	$0.828 \pm 0.082$	$73.889 \pm 31.700$	69.000	$1074.745 \pm 1060.711$
		$\mathcal{O}$ -ICID	$0.920 \pm 0.048$	$28.500 \pm 19.196$	31.000	$1.605 \pm 0.888$
	0.20	GH18	$0.794 \pm 0.058$	$107.300 \pm 24.622$	109.500	$0.005 \pm 0.003$
		GES	$0.828 \pm 0.082$	$73.889 \pm 31.700$	69.000	$1074.792 \pm 1059.921$
		$\mathcal{O}$ -ICID	$0.911 \pm 0.101$	$23.500 \pm 23.904$	20.000	$1.945 \pm 0.941$
	0.40	GH18	$0.585 \pm 0.074$	$202.000 \pm 40.877$	215.000	$0.004 \pm 0.001$
		GES	$0.828 \pm 0.082$	$73.889 \pm 31.700$	69.000	$1074.323 \pm 1060.670$
		$\mathcal{O}$ -ICID	$0.964 \pm 0.082$	$12.400 \pm 23.081$	2.000	$2.512 \pm 1.227$
	0.80	GH18	$0.320 \pm 0.036$	$362.500 \pm 36.035$	377.500	$0.004 \pm 0.002$
		GES	$0.828 \pm 0.082$	$73.889 \pm 31.700$	69.000	$1074.660 \pm 1061.174$
		$\mathcal{O}$ -ICID	$0.940 \pm 0.048$	$18.800 \pm 17.364$	10.000	$3.092 \pm 0.586$
	1.00	GH18	$0.263 \pm 0.035$	$412.400 \pm 32.925$	412.000	$0.004 \pm 0.000$
		GES	$0.828 \pm 0.082$	$73.889 \pm 31.700$	69.000	$1073.877 \pm 1060.595$
		$\mathcal{O}$ -ICID	$0.884 \pm 0.072$	$25.900 \pm 15.409$	26.500	$3.248 \pm 0.824$

Table 6: Results of causal structure learning from inverse covariance matrices in the EV case ( $\lambda = 0$ ) and the NV cases ( $\lambda > 0$ ). The scaling parameter  $\lambda$  is defined in (12).

G	$\lambda$	Algorithm	TPR	SHD	Median SHD	time (seconds)
ER3	0.00	GH18	1.000 $\pm$ 0.000	0.000 $\pm$ 0.000	0.000	0.004 $\pm$ 0.000
		GES	0.663 $\pm$ 0.042	215.000 $\pm$ 53.740	215.000	72466.820 $\pm$ 10675.060
		$\mathcal{O}$ -ICID	0.733 $\pm$ 0.114	109.600 $\pm$ 44.890	106.500	2.526 $\pm$ 0.582
	0.10	GH18	0.945 $\pm$ 0.030	67.800 $\pm$ 51.352	47.000	0.006 $\pm$ 0.004
		fastGES	0.802 $\pm$ 0.064	314.200 $\pm$ 41.590	315.500	2.527 $\pm$ 0.432
		$\mathcal{O}$ -ICID	0.867 $\pm$ 0.067	65.000 $\pm$ 33.113	57.500	2.133 $\pm$ 0.791
	0.20	GH18	0.768 $\pm$ 0.094	236.900 $\pm$ 80.733	242.500	0.005 $\pm$ 0.002
		fastGES	0.802 $\pm$ 0.064	314.200 $\pm$ 41.590	315.500	2.378 $\pm$ 0.475
		$\mathcal{O}$ -ICID	0.849 $\pm$ 0.117	76.600 $\pm$ 58.043	62.000	2.761 $\pm$ 1.151
	0.40	GH18	0.501 $\pm$ 0.068	424.200 $\pm$ 66.406	411.500	0.005 $\pm$ 0.003
		fastGES	0.802 $\pm$ 0.064	314.200 $\pm$ 41.590	315.500	2.432 $\pm$ 0.637
		$\mathcal{O}$ -ICID	0.910 $\pm$ 0.078	66.400 $\pm$ 55.191	53.000	3.415 $\pm$ 0.509
	0.80	GH18	0.229 $\pm$ 0.034	641.100 $\pm$ 65.467	635.500	0.005 $\pm$ 0.003
		fastGES	0.802 $\pm$ 0.064	314.200 $\pm$ 41.590	315.500	2.462 $\pm$ 0.531
		$\mathcal{O}$ -ICID	0.862 $\pm$ 0.082	93.400 $\pm$ 29.444	94.500	3.950 $\pm$ 0.645
	1.00	GH18	0.176 $\pm$ 0.040	703.400 $\pm$ 54.271	703.000	0.005 $\pm$ 0.003
		fastGES	0.802 $\pm$ 0.064	314.200 $\pm$ 41.590	315.500	2.382 $\pm$ 0.439
		$\mathcal{O}$ -ICID	0.705 $\pm$ 0.153	88.100 $\pm$ 22.293	86.500	3.627 $\pm$ 0.943

In addition to the results on ER1 and ER3 sets (Figure 2), the following figure (Figure 6) shows the results on the ER2 set.



(a) ER2

Figure 6: Causal structure learning by  $\mathcal{O}$ -ICID compared to GH18 and GES. The X-axis indicates the scaling parameter  $\lambda \in [0, 1]$  in (12). The true DAGs are drawn from the ER2 set with  $d = 50$  nodes.

**Same experiment on SF graphs.** The experiment of Section 4.3 is also conducted with random DAGs drawn from the SF sets. The results are presented in Figure 7 and Table 7. In particular, GES is tested only with  $\lambda = 0$  (due to running time limits), and its scores for the other values of  $\lambda$  remain the same as  $\lambda = 0$  in view of the invariance

of GES to the value of  $\lambda$  (note that  $\lambda$  only controls the scaling of each  $X_i$ 's samples). Therefore the running time of GES is only reported for  $\lambda = 0$  in Table 7.

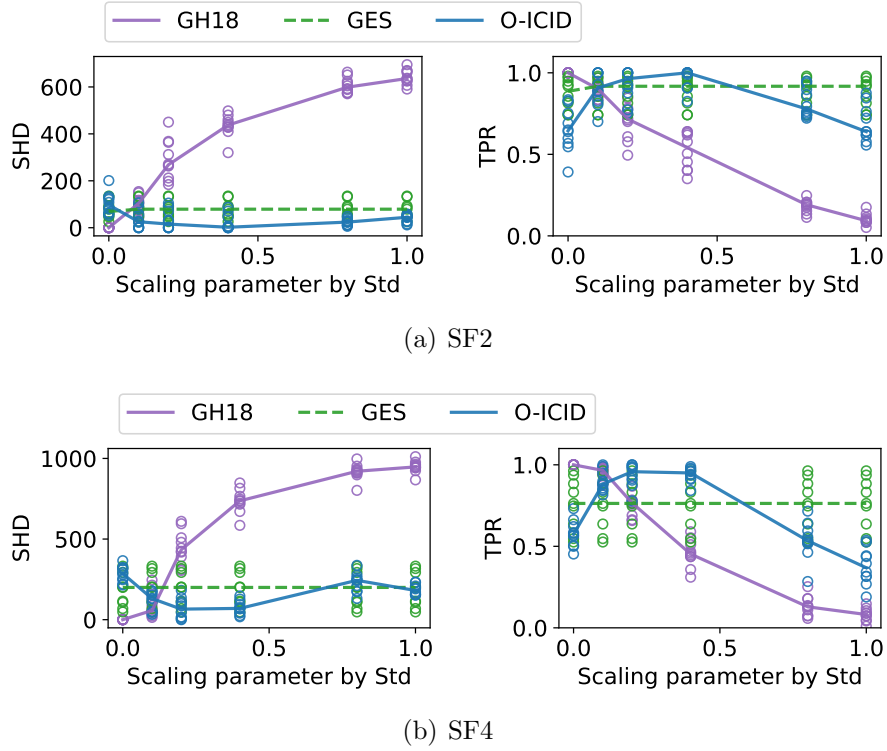


Figure 7: Causal structure learning by  $\mathcal{O}$ -ICID compared to GH18 and GES. The X-axis indicates  $\lambda \in [0, 1]$  in (12). The true DAGs are drawn from the SF2 and SF4 sets with  $d = 50$  nodes.

Table 7: Results of causal structure learning from inverse covariance matrices in the EV case ( $\lambda = 0$ ) and the NV cases ( $\lambda > 0$ ). The scaling parameter  $\lambda$  is defined in (12). The true DAGs are drawn from the SF sets. In particular, GES is tested only with  $\lambda = 0$ .

G	$\lambda$	Algorithm	TPR	SHD	Median SHD	time (seconds)
SF2	0.00	GH18	1.000 $\pm$ 0.000	0.000 $\pm$ 0.000	0.000	0.005 $\pm$ 0.001
		GES	0.877 $\pm$ 0.093	78.556 $\pm$ 37.627	79.000	742.761 $\pm$ 281.321
		$\mathcal{O}$ -ICID	0.649 $\pm$ 0.135	103.300 $\pm$ 44.697	97.000	10.445 $\pm$ 1.617
	0.10	GH18	0.897 $\pm$ 0.045	97.600 $\pm$ 38.390	104.000	0.004 $\pm$ 0.000
		GES	0.877 $\pm$ 0.093	78.556 $\pm$ 37.627	79.000	NA
		$\mathcal{O}$ -ICID	0.903 $\pm$ 0.103	38.400 $\pm$ 41.097	25.500	8.523 $\pm$ 3.172
	0.20	GH18	0.696 $\pm$ 0.106	288.800 $\pm$ 85.036	268.500	0.003 $\pm$ 0.000
		GES	0.877 $\pm$ 0.093	78.556 $\pm$ 37.627	79.000	NA
		$\mathcal{O}$ -ICID	0.924 $\pm$ 0.096	33.200 $\pm$ 41.335	15.500	6.136 $\pm$ 3.583
	0.40	GH18	0.522 $\pm$ 0.113	434.900 $\pm$ 48.045	437.500	0.003 $\pm$ 0.000
		GES	0.877 $\pm$ 0.093	78.556 $\pm$ 37.627	79.000	NA
		$\mathcal{O}$ -ICID	0.963 $\pm$ 0.062	21.600 $\pm$ 33.533	2.000	6.801 $\pm$ 3.615
	0.80	GH18	0.181 $\pm$ 0.039	606.200 $\pm$ 32.155	599.000	0.003 $\pm$ 0.000
		GES	0.877 $\pm$ 0.093	78.556 $\pm$ 37.627	79.000	NA
		$\mathcal{O}$ -ICID	0.815 $\pm$ 0.088	23.300 $\pm$ 13.483	24.000	8.691 $\pm$ 2.169
	1.00	GH18	0.102 $\pm$ 0.033	641.600 $\pm$ 31.697	636.000	0.003 $\pm$ 0.000
		GES	0.877 $\pm$ 0.093	78.556 $\pm$ 37.627	79.000	NA
		$\mathcal{O}$ -ICID	0.686 $\pm$ 0.111	37.800 $\pm$ 16.075	44.500	8.517 $\pm$ 2.748
SF4	0.00	GH18	1.000 $\pm$ 0.000	0.000 $\pm$ 0.000	0.000	0.003 $\pm$ 0.000
		GES	0.760 $\pm$ 0.161	187.222 $\pm$ 108.545	200.000	2407.557 $\pm$ 1876.750
		$\mathcal{O}$ -ICID	0.577 $\pm$ 0.082	283.300 $\pm$ 48.847	286.000	9.755 $\pm$ 2.319
	0.10	GH18	0.951 $\pm$ 0.041	93.100 $\pm$ 82.332	57.000	0.003 $\pm$ 0.000
		GES	0.760 $\pm$ 0.161	187.222 $\pm$ 108.545	200.000	NA
		$\mathcal{O}$ -ICID	0.896 $\pm$ 0.063	117.700 $\pm$ 56.210	131.000	10.094 $\pm$ 1.770
	0.20	GH18	0.751 $\pm$ 0.064	448.700 $\pm$ 103.395	434.000	0.003 $\pm$ 0.000
		GES	0.760 $\pm$ 0.161	187.222 $\pm$ 108.545	200.000	NA
		$\mathcal{O}$ -ICID	0.936 $\pm$ 0.071	69.400 $\pm$ 63.533	65.500	9.070 $\pm$ 3.105
	0.40	GH18	0.457 $\pm$ 0.083	734.500 $\pm$ 72.529	737.000	0.003 $\pm$ 0.000
		GES	0.760 $\pm$ 0.161	187.222 $\pm$ 108.545	200.000	NA
		$\mathcal{O}$ -ICID	0.941 $\pm$ 0.043	71.100 $\pm$ 42.344	70.000	9.676 $\pm$ 2.179
	0.80	GH18	0.132 $\pm$ 0.059	917.300 $\pm$ 49.218	920.500	0.003 $\pm$ 0.001
		GES	0.760 $\pm$ 0.161	187.222 $\pm$ 108.545	200.000	NA
		$\mathcal{O}$ -ICID	0.536 $\pm$ 0.114	230.000 $\pm$ 58.752	244.000	10.670 $\pm$ 3.277
	1.00	GH18	0.080 $\pm$ 0.040	947.900 $\pm$ 37.063	947.500	0.003 $\pm$ 0.000
		GES	0.760 $\pm$ 0.161	187.222 $\pm$ 108.545	200.000	NA
		$\mathcal{O}$ -ICID	0.377 $\pm$ 0.111	185.300 $\pm$ 31.245	181.000	9.124 $\pm$ 1.707

**Misspecification of noise variances.** The following figures show the sensitivity of  $\mathcal{O}$ -ICID under misspecification of noise variances in all tested configurations: the random DAGs are drawn from ER $k$  sets with  $k \in \{1, 2, 3\}$ , and the scaling parameter  $\lambda$  via standardization ranges in  $\{0.1, 0.2, 0.4, 0.8, 1.0\}$ .



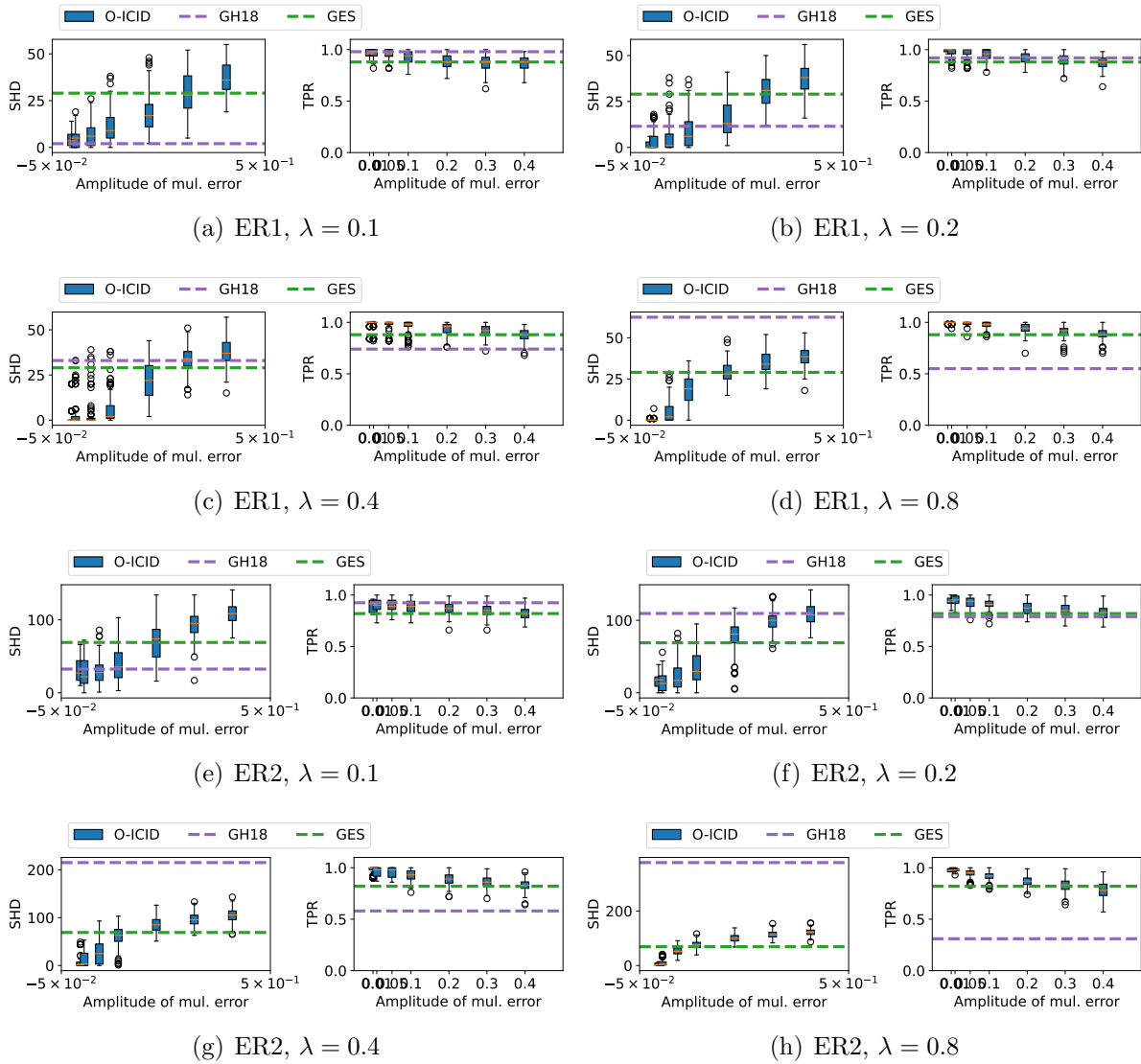


Figure 8: Causal structure learning by  $\mathcal{O}$ -ICID. The X-axis indicates the amplitude  $\sigma_\epsilon$  of average misspecifications of  $D^*$ .

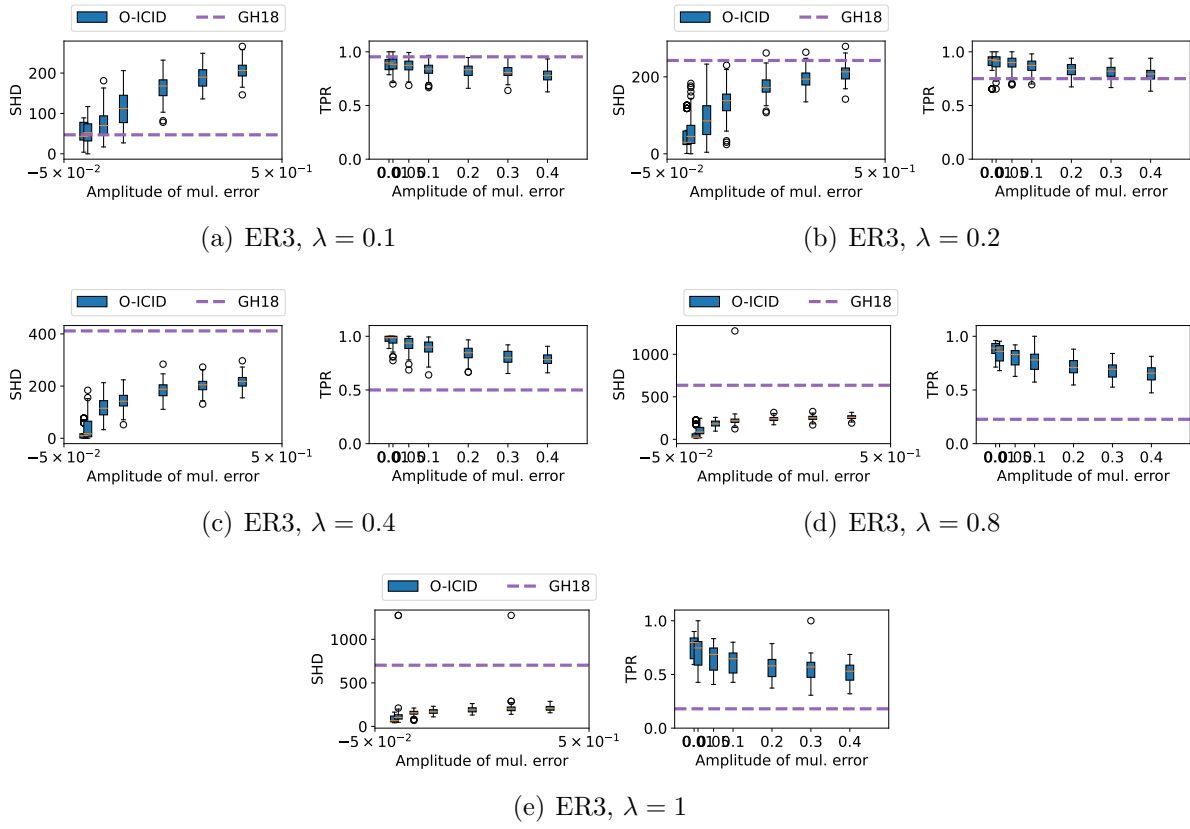


Figure 9: Causal structure learning by  $\mathcal{O}$ -ICID. The X-axis indicates the amplitude  $\sigma_\epsilon$  of average misspecifications of  $D^*$ .

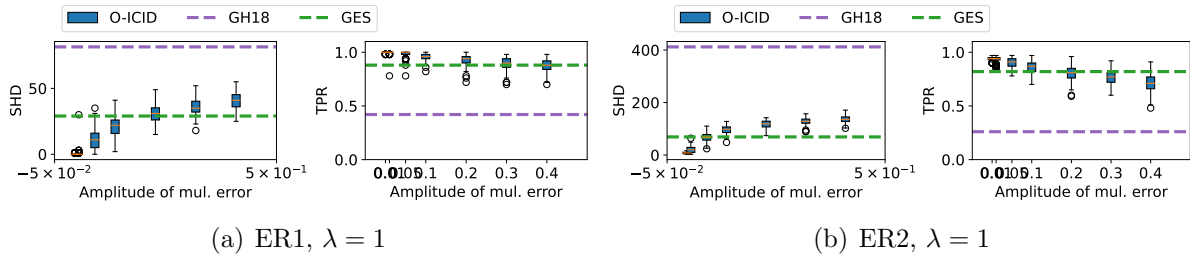


Figure 10: Causal structure learning by  $\mathcal{O}$ -ICID. The X-axis indicates the amplitude  $\sigma_\epsilon$  of average misspecifications of  $D^*$ .

## References

Bryon Aragam, Arash Amini, and Qing Zhou. Globally optimal score-based learning of directed acyclic graphs in high-dimensions. *Advances in Neural Information Processing Systems*, 32, 2019.

- Martin Arjovsky, Léon Bottou, Ishaan Gulrajani, and David Lopez-Paz. Invariant risk minimization. *arXiv preprint arXiv:1907.02893*, 2019.
- Albert-László Barabási and Réka Albert. Emergence of scaling in random networks. *science*, 286(5439):509–512, 1999.
- Amir Beck and Marc Teboulle. A fast iterative shrinkage-thresholding algorithm for linear inverse problems. *SIAM journal on imaging sciences*, 2(1):183–202, 2009.
- D. P. Bertsekas. *Nonlinear programming*, volume 2nd Editio. 1999. ISBN 1886529000. URL <http://www.citeulike.org/group/4340/article/1859441>.
- Richard B Buxton, Eric C Wong, and Lawrence R Frank. Dynamics of blood flow and oxygenation changes during brain activation: the balloon model. *Magnetic resonance in medicine*, 39(6):855–864, 1998.
- Emmanuel Candes and Terence Tao. The Dantzig selector: Statistical estimation when  $p$  is much larger than  $n$ . *The annals of Statistics*, 35(6):2313–2351, 2007.
- Wenyu Chen, Mathias Drton, and Y Samuel Wang. On causal discovery with an equal-variance assumption. *Biometrika*, 106(4):973–980, 2019.
- David Maxwell Chickering. Learning bayesian networks is NP-complete. *Learning from data: Artificial intelligence and statistics V*, pages 121–130, 1996.
- David Maxwell Chickering. Learning equivalence classes of bayesian-network structures. *The Journal of Machine Learning Research*, 2:445–498, 2002a.
- David Maxwell Chickering. Optimal structure identification with greedy search. *Journal of machine learning research*, 3(Nov):507–554, 2002b.
- Shuyu Dong and Michèle Sebag. From graphs to DAGs: a low-complexity model and a scalable algorithm. In *Joint European Conference on Machine Learning and Knowledge Discovery in Databases*, pages 107–122. Springer, 2022.
- Jerome Friedman, Trevor Hastie, and Robert Tibshirani. Sparse inverse covariance estimation with the graphical lasso. 2007. URL <http://statweb.stanford.edu/~tibs/ftp/graph.pdf>.
- Karl J Friston, Lee Harrison, and Will Penny. Dynamic causal modelling. *Neuroimage*, 19(4):1273–1302, 2003.
- Delbert Fulkerson and Oliver Gross. Incidence matrices and interval graphs. *Pacific journal of mathematics*, 15(3):835–855, 1965.
- Ming Gao, Wai Ming Tai, and Bryon Aragam. Optimal estimation of gaussian dag models. In *International Conference on Artificial Intelligence and Statistics*, pages 8738–8757. PMLR, 2022.

- AmirEmad Ghassami, Alan Yang, Negar Kiyavash, and Kun Zhang. Characterizing distribution equivalence and structure learning for cyclic and acyclic directed graphs. In *International Conference on Machine Learning*, pages 3494–3504. PMLR, 2020.
- Asish Ghoshal and Jean Honorio. Learning linear structural equation models in polynomial time and sample complexity. In *International Conference on Artificial Intelligence and Statistics*, pages 1466–1475. PMLR, 2018.
- Isabelle Guyon, Alexander R. Statnikov, and Berna Bakir Batu, editors. *Cause Effect Pairs in Machine Learning*. Springer, 2019. ISBN 978-3-030-21809-6. doi: 10.1007/978-3-030-21810-2. URL <https://doi.org/10.1007/978-3-030-21810-2>.
- Aapo Hyvärinen and Stephen M Smith. Pairwise likelihood ratios for estimation of non-gaussian structural equation models. *The Journal of Machine Learning Research*, 14(1):111–152, 2013.
- Daphne Koller and Nir Friedman. *Probabilistic graphical models: principles and techniques*. MIT press, 2009.
- Po-Ling Loh and Peter Bühlmann. High-dimensional learning of linear causal networks via inverse covariance estimation. *The Journal of Machine Learning Research*, 15(1):3065–3105, 2014.
- Romain Lopez, Jan-Christian Hütter, Jonathan Pritchard, and Aviv Regev. Large-scale differentiable causal discovery of factor graphs. *Advances in Neural Information Processing Systems*, 35:19290–19303, 2022.
- Christopher Meek. Causal inference and causal explanation with background knowledge. In *Proceedings of the Eleventh Conference on Uncertainty in Artificial Intelligence, UAI’95*, page 403–410. Morgan Kaufmann Publishers Inc., 1995. ISBN 1558603859.
- Ignavier Ng, AmirEmad Ghassami, and Kun Zhang. On the role of sparsity and DAG constraints for learning linear DAGs. *Advances in Neural Information Processing Systems*, 33:17943–17954, 2020.
- Ignavier Ng, Yujia Zheng, Jiji Zhang, and Kun Zhang. Reliable causal discovery with improved exact search and weaker assumptions. *Advances in Neural Information Processing Systems*, 34:20308–20320, 2021.
- Vern I Paulsen, Stephen C Power, and Roger R Smith. Schur products and matrix completions. *Journal of functional analysis*, 85(1):151–178, 1989.
- Judea Pearl. *Causality: Models, Reasoning and Inference*. Cambridge University Press, 2000.
- Jonas Peters, Peter Bühlmann, and Nicolai Meinshausen. Causal inference by using invariant prediction: identification and confidence intervals. *Journal of the Royal Statistical Society. Series B (Statistical Methodology)*, pages 947–1012, 2016.

- Jonas Peters, Dominik Janzing, and Bernhard Schölkopf. *Elements of causal inference: foundations and learning algorithms*. The MIT Press, 2017.
- Joseph Ramsey, Madelyn Glymour, Ruben Sanchez-Romero, and Clark Glymour. A million variables and more: the fast greedy equivalence search algorithm for learning high-dimensional graphical causal models, with an application to functional magnetic resonance images. *International journal of data science and analytics*, 3:121–129, 2017.
- Garvesh Raskutti and Caroline Uhler. Learning directed acyclic graph models based on sparsest permutations. *Stat*, 7(1):e183, 2018.
- Alexander Reisach, Christof Seiler, and Sebastian Weichwald. Beware of the simulated DAG! Causal discovery benchmarks may be easy to game. *Advances in Neural Information Processing Systems*, 34:27772–27784, 2021.
- Thomas Richardson. A polynomial-time algorithm for deciding markov equivalence of directed cyclic graphical models. In *Proceedings of the Twelfth International Conference on Uncertainty in Artificial Intelligence*, UAI’96, page 462–469, San Francisco, CA, USA, 1996. Morgan Kaufmann Publishers Inc. ISBN 155860412X.
- Donald J Rose. Triangulated graphs and the elimination process. *Journal of Mathematical Analysis and Applications*, 32(3):597–609, 1970.
- Axel Sauer and Andreas Geiger. Counterfactual generative networks. In *International Conference on Learning Representations (ICLR)*, 2021.
- Shohei Shimizu, Patrik O Hoyer, Aapo Hyvärinen, and Antti Kerminen. A linear non-Gaussian acyclic model for causal discovery. *Journal of Machine Learning Research*, 7(10), 2006.
- Shohei Shimizu, Takanori Inazumi, Yasuhiro Sogawa, Aapo Hyvärinen, Yoshinobu Kawahara, Takashi Washio, Patrik O Hoyer, and Kenneth Bollen. DirectLiNGAM: A direct method for learning a linear non-Gaussian structural equation model. *The Journal of Machine Learning Research*, 12:1225–1248, 2011.
- Stephen M Smith, Karla L Miller, Gholamreza Salimi-Khorshidi, Matthew Webster, Christian F Beckmann, Thomas E Nichols, Joseph D Ramsey, and Mark W Woolrich. Network modelling methods for fmri. *Neuroimage*, 54(2):875–891, 2011.
- Liam Solus, Yuhao Wang, and Caroline Uhler. Consistency guarantees for greedy permutation-based causal inference algorithms. *Biometrika*, 108(4):795–814, 2021.
- Peter Spirtes, Clark N Glymour, Richard Scheines, and David Heckerman. *Causation, prediction, and search*. MIT press, 2000.
- Stratis Tsirtsis, Amir-Hossein Karimi, Ana Lucic, Manuel Gomez-Rodriguez, Isabel Valera, and Hima Lakkaraju. ICML workshop on algorithmic recourse. 2021.

Lieven Vandenberghe and Martin S. Andersen. Chordal graphs and semidefinite optimization. *Foundations and Trends® in Optimization*, 1(4):241–433, 2015. ISSN 2167-3888. doi: 10.1561/2400000006. URL <http://dx.doi.org/10.1561/2400000006>.

Gherardo Varando. Learning dags without imposing acyclicity. *arXiv preprint arXiv:2006.03005*, 2020.

Xun Zheng, Bryon Aragam, Pradeep K Ravikumar, and Eric P Xing. DAGs with NO TEARS: Continuous optimization for structure learning. In *Advances in Neural Information Processing Systems*, volume 31, 2018. URL <https://proceedings.neurips.cc/paper/2018/file/e347c51419ffb23ca3fd5050202f9c3d-Paper.pdf>.